nature chemical biology

SUPPLEMENTARY INFORMATION

https://doi.org/10.1038/s41589-018-0004-9

In the format provided by the authors and unedited.

A robotic multidimensional directed evolution approach applied to fluorescent voltage reporters

Kiryl D. Piatkevich[1,17], Erica E. Jung[1,17], Christoph Straub[2], Changyang Linghu[1,3], Demian Park[1], Ho-Jun Suk[1,4], Daniel R. Hochbaum[2], Daniel Goodwin[1], Eftychios Pnevmatikakis[5], Nikita Pak[1,6], Takashi Kawashima[7], Chao-Tsung Yang[7], Jeffrey L. Rhoades[8], Or Shemesh[1], Shoh Asano[1], Young-Gyu Yoon[1,3], Limor Freifeld[1], Jessica L. Saulnier[2], Clemens Riegler[9,10], Florian Engert[9], Thom Hughes[11], Mikhail Drobizhev[11], Balint Szabo[12], Misha B. Ahrens[7], Steven W. Flavell[8], Bernardo L. Sabatini[2] and Edward S. Boyden[1,13,14,15,16]*

[1]Media Lab, Massachusetts Institute of Technology (MIT), Cambridge, MA, USA. [2]Howard Hughes Medical Institute, Department of Neurobiology, Harvard Medical School, Boston, MA, USA. [3]Department of Electrical Engineering and Computer Science, MIT, Cambridge, MA, USA. [4]Harvard-MIT Division of Health Sciences and Technology, MIT, Cambridge, MA, USA. [5]Simons Center Data Analysis, Simons Foundation, New York, NY, USA. [6]Department of Mechanical Engineering, MIT, Cambridge, MA, USA. [7]Janelia Research Campus, Howard Hughes Medical Institute, Ashburn, Virginia, USA. [8]Picower Institute for Learning & Memory and Department of Brain & Cognitive Sciences, MIT, Cambridge, MA, USA. [9]Department of Molecular and Cellular Biology and Center for Brain Science, Harvard University, Cambridge, MA, USA. [10]Department of Neurobiology, Faculty of Life Sciences, University of Vienna, Wien, Austria. [11]Department of Cell Biology and Neuroscience, Montana State University, Bozeman, Montana, USA. [12]Department of Biological Physics, Eotvos University, Budapest, Hungary. [13]Department of Biological Engineering, MIT, Cambridge, MA, USA. [14]MIT Center for Neurobiological Engineering, MIT, Cambridge, MA, USA. [15]Department of Brain and Cognitive Sciences, MIT, Cambridge, MA, USA. [16]MIT McGovern Institute for Brain Research, MIT, Cambridge, MA, USA. [17]These authors contributed equally: Kiryl D. Piatkevich and Erica E. Jung. *e-mail: esb@media.mit.edu

A robotic multidimensional directed evolution approach applied to fluorescent voltage reporters

Supplementary Information

Supplementary Table 1. Characteristics of genetically encoded fluorescent voltage reporters.

Sensor	Brightness[a]	ΔF/F (%)		On kinetics (-70 to +30mV)			Off kinetics (+30 to -70mV)			Optical response linearity to voltage changes (-100 to +50mV)	Bleaching rate/ Conditions[e]	Photocurrents at excitation wavelength		Effect of blue illumination (450-500nm) used for optogenetic control			Sub-threshold voltage imaging (<10mV)	Voltage imaging at dendritic spine	Membrane localization (Supplementary Fig. 10 for representative images)	Ref.
		Per 100mV (-70- +30mV) voltage step[b]	Per action potential (AP)	τ_{fast} (ms)[c]	% of magnitude in τ_{fast} component[d]	τ_{slow} (ms)	τ_{fast} (ms)	% of magnitude in τ_{fast} component[d]	τ_{slow} (ms)			Steady-state photocurrent[f]	Peak of transient photocurrent[g]	Photocurrent under blue light: Steady-state photocurrent[f]	Photocurrent under blue light: Peak of transient photocurrent[g]	Sensor fluorescence change under blue light				
QuasAr1		No data available[h]	21 (640nm, 3-8W/mm^2)	0.05 in HEK cells (640nm, light intensity not specified,34°C)	94 in HEK cells	3.2 in HEK cells	0.07 in HEK cells	88 in HEK cells	1.9 in HEK cells	Linear	No data available	0pA averaged over 250ms (640nm, 3W/mm^2), not broken down into steady state and transient photocurrents		0pA averaged over 250ms (488nm, 5mW/mm^2), not broken down into steady and transient photocurrents		2% increase in red fluorescence with blue (488nm) light pulses at 5mW/mm^2 in HEK cells	No data available	No data available		[1]
QuasAr2		No data available[h]	48 (640nm, 3-8W/mm^2)	0.3 in HEK cells (640nm, light intensity not specified,34°C)	62 in HEK cells	3.2 in HEK cells	0.3 in HEK cells	73 in HEK cells	4.0 in HEK cells	Linear	0.05%/s (640nm, 3W/mm^2)	0pA averaged over 250ms (640nm, 3W/mm^2), not broken down into steady state and transient photocurrents		0pA averaged over 250ms (488nm, 5mW/mm^2), not broken down into steady and transient photocurrents		2% increase in red fluorescence with blue (488nm) light pulses at 5mW/mm^2 in HEK cells	Detection of optically induced synaptic events	Voltage imaging at single dendritic spine during optically induced back-propagating action potential		
	100 ±66 (637nm, 800mW/mm^2)	39±13 (637nm, 800mW/mm^2)		0.9 ±0.2 (637nm, 800mW/mm^2,34°C)	67	11.7 ±0.7	1.6 ±0.3	76	20 ±6		0.05%/s (637nm, 2.2W/mm^2)	0pA in HEK cells (637nm, 800mW/mm^2)	First peak current of -90pA only at the beginning of light pulse, with exponential decay lasting ~6ms; subsequent peak - of ~-40pA only at the beginning of light pulse in HEK cells[k]	0pA in HEK cells (470/20nm,15mW/mm^2)	Peak currents of -6pA only at the beginning of light pulse with exponential decay lasting for 10ms for the first and subsequent peaks in HEK cells[k]				Severe aggregation in soma and mild aggregation in processes	
Archer1		85 (655nm, 880mW/mm^2)	25-40 (655nm, 880mW/mm^2)	No data available			No data available			Linear	No data available	+5pA (655nm,880mW/mm^2)	First peak current of ~+30pA only at the beginning of light pulse with duration not specified; subsequent peak currents of ~-30pA, with duration not specified[i]	70-100pA (~480nm, light intensity not specified)	150-180pA (duration not specified)	No data available	No data available	No data available	Mild aggregation in soma and severe aggregation in processes	[2]

	103 ±51 (637nm, 800mW/mm^2)	34±8 (637nm, 800mW/mm^2)		0.6 ±0.1 (637nm,800mW/mm^2 ,34°C)	68	33 ±3	1.1 ±0.3	77	87 ±4		0.07%/s (637nm, 2.2W/mm^2)	+19pA in HEK cells (637nm, 800mW/mm^2)	First peak current of ~+10pA only at the beginning of light pulse; subsequent peak currents of ~-40pA in HEK cells[k]	+14pA in HEK cells (470/20nm,15mW/mm^2)	Peak currents of +36pA only at the beginning of light pulse with exponential decay lasting for 20ms for the first and subsequent peaks in HEK cells[k]					
Archon1	278 ±106 (637nm, 800mW/mm^2)	43±5 (637nm, 80-800mW/mm^2)[j]	30±6 (637nm, 80-800mW/mm^2)[j]	0.61 ±0.06 (637nm, 800mW/mm^2 ,34°C)	88	8.1 ±0.5	1.1 ±0.2	88	13 ±3	Linear	0.01%/s (637nm, 800mW/mm^2)	0pA in HEK cells (637nm, 800mW/mm^2)	First peak current of -33pA only at the beginning of light pulse, with exponential decay lasting <5ms; no subsequent peak currents in HEK cells[k]	0pA in HEK cells (470/20nm,15mW/mm^2)	Peak currents of -8pA only at the beginning of light pulse with exponential decay lasting for 10ms for the first and subsequent peaks in HEK cells[k]	2% increase in red fluorescence with 470/20nm light pulses at 4.8mW/mm^2	Detection of spontaneous events	No data available	Minimal aggregation in soma and no aggregation in processes	This work
Archon2	801 ±407 (637nm, 800mW/mm^2)	19±2 (637nm, 80-800mW/mm^2)[j]	18±2 (637nm, 80-800mW/mm^2)[j]	0.06 ±0.01 (637nm, 800mW/mm^2 ,34°C)	70	6.7 ±0.4	0.17 ±0.01	92	7.0 ±0.5	Linear	0.03% /s (637nm, 0.8W/mm^2)	0pA in HEK cells (637nm, 800mW/mm^2)	No peak currents in HEK cells	0pA in HEK cells (470/20nm,15mW/mm^2)	0pA in HEK cells	1% increase in red fluorescence with 470/20nm light pulses at 4.8mW/mm^2	Not tested	Voltage imaging at dendritic spines during spontaneous events	Mild aggregation in soma and no aggregation in processes	
Ace2N-mNeon		-4 (steady state), -19 (peak)[l] (505nm, 15mW/mm^2)	-12 (505nm, 15mW/mm^2)	0.36 in HEK cells (505nm, 15mW/mm^2 ,22°C)	74 in HEK cells	4.2 in HEK cells	0.42 in HEK cells	64 in HEK cells	5.2 in HEK cells	Nonlinear for steady state response; linear for peak fluorescence response	0.7%/s (505nm, 15mW/mm^2)	–0.2 ± 0.1pA (505nm,15mW/mm^2)	Peak currents of ~-10pA and ~+10pA at the beginning and the end of light pulse respectively with exponential decay lasting for ~200ms for each transient current; subsequent peak currents not specified	Same as the photocurrents measured under excitation wavelength; see data at left		Not applicable: blue light is used for voltage imaging	Detection of spontaneous events	No data available		[3]
Ace2N-4aa-mNeon		Steady-state fluorescence not specified, -9 (peak)[l] (505nm, 15mW/mm^2)	-5 (505nm, 15mW/mm^2)	0.37 in HEK cells (505nm, 15mW/mm^2 ,22°C)	58 in HEK cells	5.5 in HEK cells	0.50 in HEK cells	60 in HEK cells	5.9 in HEK cells	No data available	0.6%/s (505nm, 15mW/mm^2)	No data available		No data available		Not applicable: blue light is used for voltage imaging	No data available	No data available		
		-6 (475nm, 13mW/mm^2)[m]	-5±2 (475nm, 13mW/mm^2)[m]	2.2 ±0.1 (475nm,	61	6.4 ±0.1	3.8 ±0.1	90	17.5 ±0.7		0.13%/s (475nm, 13mW/mm^2)[n]							Mild aggregation in soma and no aggregation in processes	

				13mW/mm^2 ,34°C)[m]														
MacQ-mCitrine		-12 (505nm, 15mW/mm^2)	-5 (505nm, 15mW/mm^2)	2.8 in HEK cells (505nm, 15mW/mm^2 ,22°C)	74 in HEK cells	71 in HEK cells	5.4 in HEK cells	77 in HEK cells	67 in HEK cells	Compressed dynamic range relative to linear (no additional changes >0mV)	1.3%/s (505nm, 15mW/mm^2)	–0.2 ± 0.2 pA (505nm, 15mW/mm^2)	First peak current of +25pA only at the beginning of light pulse, with exponential decay lasting ~20ms; subsequent peak currents not specified	Same as the photocurrents measured under excitation wavelength; see data at left	Not applicable: blue light is used for voltage imaging	Detection of spontaneous events	No data available		4
ASAP1		No data available[h]	-6 (488nm, light intensity not specified)	2.1 in HEK cells (488nm, 25-50mW/mm^2 , 22°C)	60 in HEK cells	71.5 in HEK cells	2.0 in HEK cells	43 in HEK cells	50.8 in HEK cells	Bi-exponential	0.3%/s (470nm, 15mW/mm^2)	No data available		No data available	Not applicable: blue light is used for voltage imaging	Detection of spontaneous events	No data available		5

Voltage sensors tested in brain tissues (organotypic or acute brain slice) and live animals with single cell resolution are included (unless they were shown to be exceeded in specifications by a more recent reporter[5–8]); we additionally included Quasar1. Sensors highlighted in red and green have fluorophores based on opsins (excitation at ~640nm for QuasAr2, 655nm for Archer1 and 637nm for Archon1 and Archon2) and GFP-like proteins (excitation at 488-505nm), respectively. Data from references and this study were measured in neuronal culture if not specified. Some data from references were estimated from plots/traces in papers. Data highlighted in gray were obtained in this study. Numbers shown for our measurements are mean ± standard deviation. In this study, $\triangle F/F$ and on/off kinetics were measured in neuronal cultures at 32°C (n=11, 8, 10, 9, 17 neurons for QuasAr2, Archer1, Archon1, Archon2 and Ace2N-4aa-mNeon, respectively). [a]Brightness of red voltage sensors expressed in neurons were expressed as a percentage relative to QuasAr2 (i.e., 100% = QuasAr2; n=18, 16, 23, 23 neurons for QuasAr2, Archer1, Archon1 and Archon2, respectively; imaging condition, λ_{ex} = 637nm at 800mW/mm^2 and λ_{em} = 664LP for all constructs).[b]Values represent fluorescence change between baseline fluorescence at -70mV and steady-state fluorescence at +30mV during a 100mV voltage step. [c]Imaging conditions described in the τ_{fast} section were used throughout the measurement of on and off kinetics of each sensor. [d]In this study, voltage kinetics was evaluated by bi-exponential fitting, $F(t) = A\times(C\times\exp(-t/\tau_{fast})+(1-C)\times\exp(-t/\tau_{slow}))$, where C represents the % of current magnitude in τ_{fast} component**.** [e]Light intensity used for bleaching tests in this study was adjusted to have the same initial signal-to-noise ratio (SNR) of action potentials (25±8, 26±12, 26±10, 26±10 and 28±7 for Quasar2, Archer1, Archon1, Archon2 and Ace2N-4aa-mNeon, respectively; n's are as in **Fig. 2c**); see **Methods** for hardware configuration used for these experiments for each construct. [f]Steady-state value is the photocurrent during the time when the first derivative of photocurrent with respect to time reaches zero immediately after the time point of the transient peak value. [g]Transient peak value is the maximum of absolute photocurrent at the start and/or the end of illumination. [h]Data for 100 mV voltage steps was acquired only in HEK cells in the original manuscript. [i]Subsequent peak currents were measured in reference [2] by applying repetitive pulses of light with the same intensity separated by dark recovery periods of a few seconds each. Duration of peak currents was not shown in the paper. [j]Light intensity was adjusted to prevent signal saturation. $\triangle F/F$ did not depend on light intensity. [k]Subsequent peak currents were measured in this study by applying repetitive pulses of light with the same intensity separated by dark recovery periods of a few seconds each. [l]The difference in steady-state and peak fluorescence changes relative to baseline for Ace2N-mNeon and Ace2N-4aa-mNeon are due to hysteresis behavior in response to a voltage step. [m]475 nm illumination efficiently excited green fluorescence of mNeonGreen[9] in the Ace2N-4aa-mNeon fusion protein allowing a similar signal-to-noise

ratio for action potential imaging as for other voltage sensors tested in this study (see above). [n]Photobleaching rate of Ace2N-4aa-mNeonGreen measured in this study was slower than that reported in the original publication, most likely due to the slightly blue shifted excitation wavelength used for imaging (475 nm vs 505 nm)[3].

Supplementary Table 2. Performance of genetically encoded fluorescent voltage reporters in brain tissues and live animals.

Tested organism	Voltage sensor	Tested area (cell type) /Promoter/ Gene delivery	ΔF/F (%)		Signal-to-noise ratio	Continuous recording duration (as shown in the study; not a fundamental parameter)	Ability to resolve temporally close (<50ms) spikes	Subthreshold voltage imaging	Voltage imaging at processes	Ref.
			per 100mV (-70-+30mV) voltage steps[a]	per AP						
Organotypic brain slice	**QuasAr2**	Hippocampus/ CaMKIIα/ biolistic gene delivery	No data available	16	32[b] at 12W/mm^2, 1kHz	10s	Resolved spikes evoked 10--20ms apart[c]. Higher frequency not reported.	Inhibitory potentials were presented but not quantified with electrophysiology	Single-trial voltage imaging of optically-induced events at proximal dendrites	1
Acute brain slice	**Ace2N-mNeon**	Visual cortex V1 /CMV-T7/rabies SAD-ΔG	No data available	-9[c]	No data available	No data available	No data available	No data available	No data available	3
	MacQ-mCitrine	Neocortical pyramids & PV interneurons/ CAG/*In utero* electroporation	No data available	-2.5 in neocortical pyramids, -0.5 in PV interneurons	6 in neocortical pyramids, 2 in PV interneurons[d] at 30mW/mm^2, 440Hz	2s	No data available	No data available	No data available	4
	ASAP1	Layer 5 cortical pyramidal neurons/ CAG/*In utero* electroporation	No data available	-6	5-10[c] at 8-50mW/mm^2, 400Hz	<1.5s	Unable to resolve spikes evoked 20ms apart.	Unable to resolve 30mV depolarization in 25Hz AP trains (2-5ms, 600-1,500pA current pulses)	No data available	5
	Archon1	Motor cortex layer 2/3 pyramidal neurons/ CAG/*In utero* electroporation	23.5±9.3	22.4±9.4 at 1.5W/mm^2, 22.2±10.2 at 15W/mm^2, both at 1kHz	12±5 at 1.5W/mm^2, 21±11 at 15W/mm^2, both at 1kHz	30s	Resolved spikes evoked 10ms apart. Higher frequency not tested.	Single trial recording of 5mV depolarization (by 2ms, 50-200pA current injections and synaptic inputs)	Not tested	This work
	Archon2	Motor cortex layer 2/3 pyramidal neurons/ CAG/*In utero* electroporation	18.8±8.3	9.4±2.1 at 15W/mm^2	16±3 at 15W/mm^2, 1kHz	30s	Resolved spikes evoked 10ms apart. Higher frequency not tested.	Single trial recording of 7mV depolarization (by 2ms, 50-200pA current injections and synaptic inputs)	Not tested	
In vivo C. elegans	**Archer1**	AWC neuron /*pstr-2*/ transgenic line	No data available	0.4	<5[c] at 880mW/mm^2, 250Hz	40s	Not applicable	No data available	No data available	2

	Archon1	AVA neuron /*rig-3*/ transgenic line	No data available	22±4	30±10 at 800mW/mm^2, 33Hz	960s	Not applicable	No data available	Single-trial voltage imaging of spontaneous events in an axon	This work
In vivo Drosophila	**Ace2N-2aa-mNeon**	Olfactory neurons /Gal4-UAS, Hsp70/ transgenic line	No data available	-2[c]	10-15[c] at 20mW/mm^2,1kHz	3s	Resolved spikes evoked 10--20ms apart[c]. Higher frequency not reported.	No data available	Single trial voltage imaging of stimulus-driven events at axon and dendrites	[3]
	ASAP2f	Various areas and cell types /various promoters/ transgenic line	No data available	(-5)-(-10) depending on cell types	No data available	600s	No data available	No data available	Single-trial voltage imaging of stimulus-driven events at axon and dendrites	[10]
In vivo zebra fish	**Archon1**	Random subset of neurons/ Gal4-UAS, β-actin/ transient expression	No data available	33±6	16±10 at 2.2W/mm^2, 500Hz, 333Hz	300s	Resolved spikes evoked 10ms apart. Higher frequency not tested.	Detection of subthreshold peaks	Single-trial voltage imaging of spontaneous events in an axon	This work
In vivo mouse	**ACE2N-4aa-mNeon**	Layer 2/3 visual cortical neurons/ CMV-T7/rabies SAD-ΔG	No data available	-3[c]	5-10[c] at 25mW/mm^2,1kHz	30s	Resolved spikes evoked 10--20ms apart[c]. Higher frequency not reported.	Detection of baseline fluctuation	Multi-trial voltage imaging of interrogated events at proximal dendrites (spike-triggered averages of 1900 spikes)	[3]
	MacQ-mCitrine	Purkinje neurons/ CAG/*In utero* electroporation	No data available	-1.5[c]	5-10[c] at 10mW/mm^2, 190Hz	<30s	No data available	No data available	No data available	[4]

Sensors from **Supp Table 1a**, excluding Quasar1 since it was not used in intact brain tissues, and including ASAP2f which had been used in Drosophila but not extensively characterized in cultured cells. Sensors highlighted with red and green have fluorophores based on opsins (excitation at ~637nm) and GFP-like proteins (excitation at 488-505nm), respectively. Some data from references was estimated from plots/traces in the papers. Data highlighted with gray was obtained in this study. Numbers shown for our measurements are mean ± standard deviation. [a]Values represent fluorescence change between baseline fluorescence at -70mV and steady-state fluorescence at +30mV during 100mV voltage steps. [b]Method to calculate SNR was not specified in the paper. [c]Estimated from traces presented in the corresponding paper. [d]SNR defined as $\Delta F/F \times \sqrt{\bar{F}}$, where $\bar{F}$ is a pixel's mean baseline fluorescence emission rate.

Supplementary Table 3. Screening conditions for monomeric near-infrared fluorescent proteins (FPs) and Arch-based voltage sensors.

Template protein	Mutagenesis	Library size (independent clones)	FACS enrichment[a]		Imaging conditions
			Channel 1	Channel 2	
*Rp*BphP1	Site-directed	$1.29 \cdot 10^6$	Ex: 640 nm; Em: 670/30BP	Ex: 640 nm; Em: 710/50BP	10x 0.3NA; Ex: 628/31BP; Em: 716/40BP
	Random	$1.26 \cdot 10^6$			10x 0.3NA; Ex: 628/31BP; Em: 716/40BP
	Random	$4.32 \cdot 10^6$			10x 0.3NA; Ex: 628/31BP; Em: 664LP
QuasAr2	Random	$1.6 \cdot 10^6$	Ex: 640 nm; Em: 670/30BP	Ex: 640 nm; Em: 710/50BP	10x 0.3NA/40x 0.75NA[b]; Ex: 628/31BP; Em: 664LP
	Site-directed	$8.1 \cdot 10^6$			10x 0.3NA/40x 0.75NA[b]; Ex: 628/31BP; Em: 664LP

[a]Cells showing positive signals in the indicated channels were collected; see **Fig. 1a** for details.
[b]Objective lens used for protein localization screening.
Ex – excitation wavelength; Em – emission wavelength; BP – bandpass; LP – longpass.

Supplementary Table 4. Properties of bacteriophytochrome-derived FPs.

Protein	BphP template	Abs. (nm)[a]	Em. (nm)[a]	Extinction coefficient ($M^{-1}cm^{-1}$)[a]	Quantum yield (%)[a]	Molecular brightness[b] vs. iRFP (%)	pK_a	Photo-stability, $t_{1/2}$ (s)	Oligo-meric state
iRFP670	*Rp*BphP6	651	670	59,000	13.2	154	4.5	ND	Dimer
iRFP682	*Rp*BphP2	670	682	69,000	11.3	155	4.6	ND	Dimer
iRFP702	*Rp*BphP6	673	702[c]	85,000	8.2[c]	138	4.5[c]	ND	Dimer
iRFP	*Rp*BphP2	692	713	80,000	6.3[c]	100	4.5[c]	ND	Dimer
iRFP720	*Rp*BphP2	700	720[c]	70,000	6.0[c]	83	4.5[c]	ND	Dimer
mIFP[d]	*Br*BphP	683	703	82,000	8.4	137	3.5[e]	227	Monomer
miRFP670[f]	*Rp*BphP1	642	670	87,400	14	243	4.5	ND	Monomer
miRFP703[f]	*Rp*BphP1	674	703	90,900	8.6	155	4.5	ND	Monomer
miRFP709[f]	*Rp*BphP1	683	709	78,400	5.4	84	4.5	ND	Monomer
miRFP	*Rp*BphP1	674	703	92,400	9.7	178	4.3	432	Monomer

[a]Measured on protein purified from *E.coli*. [b]The product of molar extinction coefficient and quantum yield. All data was collected in this study, except: [c]data from ref. [11]; [d]this row of data from ref. [12]; [e]estimated from the plot in ref. [12]; [f]data from ref. [13].

ND – not determined. Proteins spectrally similar to miRFP are highlighted with grey.

Supplementary Table 5. Statistical analysis for **Figs. 1, 2, 3** and **Supplementary Figures 4, 14**.

Statistical analysis for **Fig. 1d**

Protein	Number of data points for statistics (n)	Mean	Standard error of mean
Template	16	3.0616	0.3247
Archon1	15	10.3510	1.3950
Archon2	16	7.7443	1.0947

Kruskal-Wallis Test Rank Sums

Protein	Count	Score Sum	Expected Score	Score Mean	(Mean-Mean0)/Std0
Archon1	15	510.500	360.000	34.0333	3.423
Archon2	16	449.500	384.000	28.0938	1.459
Template	16	168.000	384.000	10.5000	-4.838

1-Way Test, ChiSquare Approximation

ChiSquare	DF	Prob>ChiSq
24.9704	2	<.0001

Nonparametric Comparisons With Control Using Steel's test
Control Group: Template

q*	Alpha
2.21304	0.05

Protein1	Protein2	Score Mean Difference	Std Err Dif	Z	p-Value
Archon2	Template	-12.4375	3.316625	-3.75005	0.0003
Archon1	Template	-14.9188	3.267687	-4.56554	<0.0001

Statistical analysis for **Fig. 1g**

Protein	Number of data points for statistics (n)	Mean	Standard error of mean
Template	5	45.9002	2.0012
Archon1	6	80.6349	3.3146
Archon2	4	19.5504	0.8723

Kruskal-Wallis Test Rank Sums

Protein	Count	Score Sum	Expected Score	Score Mean	(Mean-Mean0)/Std0
Archon1	6	75.000	48.000	12.5000	3.123
Archon2	4	10.000	32.000	2.5000	-2.807
Template	5	35.000	40.000	7.0000	-0.551

1-Way Test, ChiSquare Approximation

ChiSquare	DF	Prob>ChiSq
12.3750	2	0.0021

Nonparametric Comparisons With Control Using Steel's test
Control Group: Template

q*	Alpha
2.21298	0.05

Protein1	Protein2	Score Mean Difference	Std Err Dif	Z	p-Value
Archon2	Template	4.27500	1.837117	2.32702	0.0374
Archon1	Template	-5.31667	2.008316	-2.64733	0.0155

Statistical analysis for **Fig. 2b**

Protein	Number of data points for statistics (n)	Mean	Standard error of mean
Archer1	16	534.2359	66.17127
QuasAr2	18	519.0741	80.68391
Archon1	23	1440.3283	114.8950
Archon2	23	4160.2174	441.5730

Kruskal-Wallis Test Rank Sums

Protein	Count	Score Sum	Expected Score	Score Mean	(Mean-Mean0)/Std0
Archer1	16	304.000	648.000	19.0000	-4.132
Archon1	23	1052.00	931.500	45.7391	1.276
Archon2	23	1568.00	931.500	68.1739	6.761
QuasAr2	18	316.000	729.000	17.5556	-4.753

1-Way Test, ChiSquare Approximation

ChiSquare	DF	Prob>ChiSq
65.0330	3	<.0001

Nonparametric Comparisons For All Pairs Using Steel-Dwass test

q*	Alpha
2.56903	0.05

Protein1	Protein2	Score Mean Difference	Std Err Dif	Z	p-Value
Archon2	Archon1	21.3043	3.958114	5.38245	<.0001
Archon2	Archer1	19.4470	3.711762	5.23929	<.0001
Archon1	Archer1	19.1291	3.711762	5.15364	<.0001
QuasAr2	Archer1	-2.4201	3.421575	-0.70732	0.8942
QuasAr2	Archon1	-18.2717	3.769795	-4.84688	<.0001
QuasAr2	Archon2	-20.4505	3.769795	-5.42483	<.0001

Statistical analysis for **Fig. 2h**

Wilcoxon signed-rank test between electric and optical FWHM of Archon1 in culture.

P-value	0.0156*
rank sum test statistic	14

Statistical analysis for **Fig. 2i**

Kruskal-Wallis Test Rank Sums

Protein	**Count**	**Score Sum**	**Expected Score**	**Score Mean**	**(Mean-Mean0)/Std0**
Ace	5	52.000	80.000	10.4000	-1.477
Archer1	5	77.000	80.000	15.4000	-0.134
Archon1	7	196.000	112.000	28.0000	3.945
Archon2	7	143.000	112.000	20.4286	1.441
QuasAr2	7	28.000	112.000	4.0000	-3.945

1-Way Test, ChiSquare Approximation

ChiSquare	**DF**	**Prob>ChiSq**
27.9664	4	<0.0001

Nonparametric Comparisons For All Pairs Using Steel-Dwass test

q*	**Alpha**
2.72777	0.05

Protein1	**Protein2**	**Score Mean Difference**	**Std Err Dif**	**Z**	**p-Value**
Archon1	Ace	5.82857	2.111195	2.76079	0.0456
Archon1	Archer1	5.82857	2.111195	2.76079	0.0456
Archon2	Ace	5.82857	2.111195	2.76079	0.0456
Archon2	Archer1	4.45714	2.111195	2.11119	0.2152
Archer1	Ace	4.00000	1.914854	2.08893	0.2248
QuasAr2	Ace	-5.82857	2.111195	-2.76079	0.0456
QuasAr2	Archer1	-5.82857	2.111195	-2.76079	0.0456
Archon2	Archon1	-6.85714	2.236068	-3.06661	0.0184
QuasAr2	Archon1	-6.85714	2.236068	-3.06661	0.0184
QuasAr2	Archon2	-6.85714	2.236068	-3.06661	0.0184

Statistical analysis for **Fig. 3f**

Wilcoxon signed-rank test between electrical and optical FWHM of Archon1 at 1.5W.

P-value	0.002**
rank sum test statistic	27.5

Wilcoxon signed-rank test between electrical and optical FWHM of Archon1 at 15W.

P-value	0.0002***

rank sum test statistic	45.5

Statistical analysis for **Fig. 3f**

Wilcoxon signed-rank test of Archon1 ΔF/F per action potential at 1.5W and at 15W.

P-value	0.375
rank sum test statistic	9.5

Statistical analysis for **Fig. 3f**

Wilcoxon signed-rank test of Archon1 SNR per action potential at 1.5W and at 15W.

P-value	0.002**
rank sum test statistic	-27.5

Statistical analysis for **Supplementary Figure 4**

Supplementary Figure 4c

Protein	**Number of data points for statistics (n)**	**Mean**	**Standard error of mean**
mIFP	4	29.33	0.75
miRFP	4	100.00	5.70

Wilcoxon rank sum test between mIFP and miRFP.

P-value	0.0286
rank sum test statistic	10

Supplementary Figure 4d

Protein	**Number of data points for statistics (n)**	**Mean**	**Standard error of mean**
mIFP	8	227.36	11.27
miRFP	8	432.74	25.45

Wilcoxon rank sum test between mIFP and miRFP.

P-value	1.5540e-04
rank sum test statistic	36

Statistical analysis for **Supplementary Figure 14**

(a) Membrane resistance

Kruskal-Wallis Test Rank Sums

Protein	# of cells	Score Sum	Expected Score	Score Mean	(Mean-Mean0)/Std0
Negative	10	384.000	355.000	38.4000	0.478
Archer1	8	344.000	284.000	43.0000	1.098
QuasAr2	10	275.000	355.000	27.5000	-1.334
Ace2N-4aa-mNeon	14	208.000	497.000	14.8571	-4.236
Archon1	17	719.000	603.500	42.2941	1.575
Archon2	11	555.000	390.500	50.4545	2.647

1-Way Test, ChiSquare Approximation

ChiSquare	DF	Prob>ChiSq
25.0740	5	0.0001

Nonparametric Comparisons With Control Using Steel's test
Control Group: Negative

q*	Alpha
2.50102	0.05

Protein	Score Mean Difference	Std Err Dif	Z	p-Value
Archon2	4.10455	2.711088	1.51398	0.3990
Archer1	1.68750	2.530984	0.66674	0.9394
Archon1	1.19118	3.163208	0.37657	0.9947
QuasAr2	-3.10000	2.645751	-1.17169	0.6379
Ace2N-4aa-mNeon	-8.65714	2.927700	-2.95698	0.0136

(b) Membrane capacitance

Kruskal-Wallis Test Rank Sums

Protein	# of cells	Score Sum	Expected Score	Score Mean	(Mean-Mean0)/Std0
Negative	10	268.000	355.000	26.8000	-1.452
Archer1	8	190.000	284.000	23.7500	-1.726
QuasAr2	10	375.000	355.000	37.5000	0.327
Ace2N-4aa-mNeon	14	762.000	497.000	54.4286	3.884
Archon1	17	586.500	603.500	34.5000	-0.226
Archon2	11	303.500	390.500	27.5909	-1.396

1-Way Test, ChiSquare Approximation

ChiSquare	DF	Prob>ChiSq
18.4052	5	0.0025

Nonparametric Comparisons With Control Using Steel's test
Control Group: Negative

q*	Alpha
2.50102	0.05

Protein	Score Mean Difference	Std Err Dif	Z	p-Value
Ace2n-4aa-mNeon	9.17143	2.927700	3.13264	0.0077
QuasAr2	3.30000	2.645751	1.24728	0.5825
Archon1	2.93824	3.163208	0.92888	0.8077
Archon2	0.85909	2.711088	0.31688	0.9976
Archer1	-1.68750	2.530984	-0.66674	0.9394

(3) Resting potential

Kruskal-Wallis Test Rank Sums

Protein	# of cells	Score Sum	Expected Score	Score Mean	(Mean-Mean0)/Std0
Negative	10	245.500	400.000	24.5500	-2.285
Archer1	9	453.000	360.000	50.3333	1.436
QuasAr2	10	520.000	400.000	52.0000	1.773
Ace2N-4aa-mNeon	17	536.000	680.000	31.5294	-1.722
Archon1	19	852.500	760.000	44.8684	1.062
Archon2	14	553.000	560.000	39.5000	-0.084

1-Way Test, ChiSquare Approximation

ChiSquare	DF	Prob>ChiSq
12.4210	5	0.0295

Non-parametric Comparisons With Control Using Steel's test
Control Group: Negative

q*	Alpha
2.49072	0.05

Protein	Score Mean Difference	Std Err Dif	Z	p-Value
Archon1	7.478947	3.297313	2.268194	0.0870
QuasAr2	6.600000	2.635786	2.503997	0.0483
Archer1	5.594444	2.574207	2.173269	0.1085
Archon2	4.800000	2.897632	1.656525	0.3059
Ace2N-4aa-mNeon	2.461765	3.154021	0.780516	0.8833

Supplementary Table 6. Characterization of Arch mutants with various combinations of point mutations in comparison to Archon1 and QuasAr2, in HEK293T cells.

Mutation relative to QuasAr2[a]	Membrane localization relative to QuasAr2, %	Brightness relative to QuasAr2, %	Voltage sensitivity per -70 to +30 mV step, %	Kinetics[b], ms	
				τ_{on}	τ_{off}
None (QuasAr2)	100	100	46	2.3	0.6
T20S/G41A/V44E/D88N/A137T/G242Q	348	140	47	2.4	0.8
T20S/G41A/V44E/S80P/D88N/A137T/G242Q	409	169	66	2.9	1.2
T20S/G41A/V44E/S80P/D88N/A137T/T184I/L199I/G242Q (Archon1)	312	198	81	3.6	1.7
T20S/G41A/V44E/T56P/S80P/D88N/A137T/T184I/L199I/G242Q	740	228	90	10.0	8.4
T20S/G41A/V44E/T56P/S80P/D88N/T118I/A137T/T184I/L199I/G242Q	609	253	84	10.1	8.7
T20S/G41A/V44E/T56P/S80P/D88N/A137T/T184I/L199I/A226C/G242Q	ND	ND	76	14.7	15.4
T20S/G41A/V44E/T56P/S60C/S80P/D88N/A137T/T184I/L199I/G242Q	264	253	63	9.1	6.2
T20S/G41A/V44E/S60C/S80P/D88N/A137T/T184I/L199I/G242Q	361	211	74	3.6	1.5
T20S/G41A/V44E/S60C/S80P/D88N/T118I/A137T/T184I/L199I/G242Q	266	194	ND	ND	ND
T20S/G41A/V44E/S80P/D88N/A137T/T184I/P196S/L199I/G242Q	214	187	ND	ND	ND
T20I/G41A/V44E/S80P/D88N/A137T/T184I/L199I/G242Q	202	139	ND	ND	ND
T20I/G41A/V44E/S80P/D88N/T118I/A137T/T184I/L199I/G242Q	195	119	ND	ND	ND

[a]amino acid numbering following that of aR2, see **Supplementary Figure 11**; [b]τ_{on} and τ_{off} are defined as the time between the onset of the fluorescence rise and fall, respectively, and the time the fluorescence reaches half of the final amplitude. ND, not determined. The values are calculated by a custom script in MATLAB.

Supplementary Figure 1. Optimization of calcium phosphate transfection conditions for expression of gene libraries in HEK293T cells.

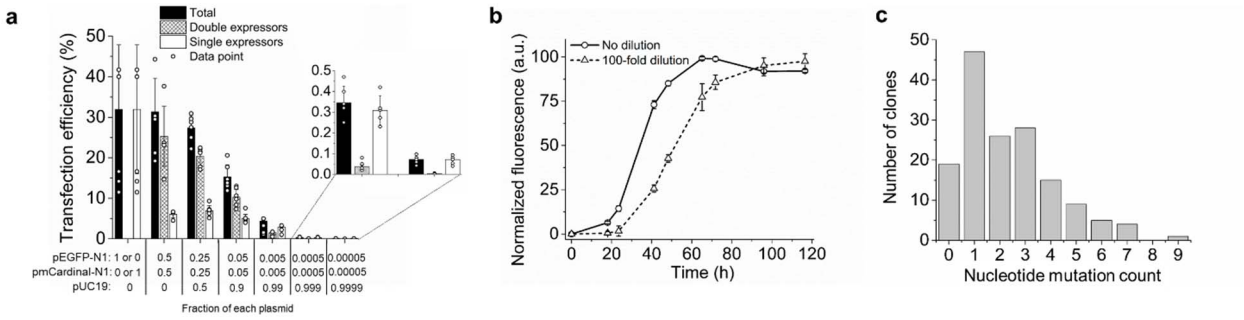

d

Plasmid	Amount of plasmid per well of 24-well plate (ng), by ratio condition (as in panel **a**)							
	1:0:0	0:1:0	0.5:0.5:0	0.25:0.25:0.5	0.05:0.05:0.9	0.005:0.005:0.99	0.0005:0.0005:0.999	0.00005:0.00005:0.9999
pEGFP-N1	700	0	350	175	35	3.5	0.35	0.035
pmCardinal-N1	0	700	350	175	35	3.5	0.35	0.035
pUC19	0	0	0	350	630	693	699.3	699.93

(**a**) For expression of gene libraries in mammalian cells, we had to create a way of transfecting single genes into cultured cells, so that high-content imaging and subsequent genotyping of individual cells would be meaningful. Electroporation[14,15] and transduction[16,17] have been used to deliver single genes into single cells in bulk, but we considered whether commonly used chemical means might offer greater degrees of simplicity and scalability. We chose calcium phosphate transfection due to the flexibility of adjusting the amount of DNA delivered across many orders of magnitude, in comparison to other chemical means[18,19]. To validate the potential for single gene-per-cell transfection, we delivered to cultured HEK293T cells an equimolar mixture of plasmids encoding green (EGFP) and red (mCardinal) fluorescent proteins (FPs), diluted by varying amounts of empty pUC19 plasmid, using a commercially available calcium phosphate transfection kit according to a slightly modified manufacturer's protocol (see **Online Methods**). As an expression vector, we used commercially available pN1 plasmid (Clontech), which can be replicated in HEK293T cells due to the SV40 origin of replication, thus enhancing expression of target genes[20]. We then analyzed the cells via flow cytometry to access the fraction of the cells that expressed only one of the two transfected FPs. We then plotted transfection efficiency of a series of DNA mixtures containing pEGFP-N1, pmCardinal-N1 and pUC19 plasmids in ratios 1:0:0, 0:1:0, 0.5:0.5:0, 0.25:0.25:0.5, 0.05:0.05:0.9, 0.005:0.005:0.99, 0.0005:0.0005:0.999, and 0.00005:0.00005:0.9999, respectively, upon delivery into HEK293T cells using our calcium phosphate protocol; panel **a** shows transfection efficiency (percentage of FP-expressing cells; *black bars*, "Total"), including cells expressing both FPs (*cross hatched bars*, "Double expressors") and just one FP (either EGFP or mCardinal; *open bars*, "Single expressors"; n = 5-6 transfected samples from two cultures; columns, mean; error bars, standard deviation (SD)). With dilution factors of 100, 1,000, and 10,000, respectively, cells with just one of the fluorophores were ~2x, ~8x, and ~23x more common than dual expressors, with 4.4±0.8%, 0.35±0.8% and 0.07±0.02% (all numbers mean ± standard deviation (SD); n = 6 experiments on 2 different days) transfection

efficiency as defined by the fraction of cells expressing either or both of the two fluorophores. Accordingly, we used 100x dilution throughout the paper, to balance the single cell transfection ratio and efficiency for all screens. (**b**) In order to evaluate optimal duration of gene library expression for screening, we compared the kinetics of EGFP expression in HEK293T cells upon transfection with and without 100-fold plasmid dilution. The peak of protein expression for 100-fold diluted pEGFP-N1 plasmid was reached in 100-110 h after transfection, which is about 40 h slower than that for the non-diluted plasmid. Panel **b** demonstrates kinetics of EGFP expression in HEK293T cells upon calcium phosphate transfection of pEGFP-N1 plasmid with no dilution (*open circles, solid line*; n = 4 transfected samples from the same culture passage) and 100-fold dilution with pUC19 plasmid (*open triangles*, *dashed line*; n = 4 transfected samples from the same culture passage). The 0 time point corresponds to the time of the transfection performed. Open symbols, mean; error bars, SD. Therefore, all further library enrichments by FACS were performed at least in 48 h post transfection. (**c**) To determine the impact of single-copy dilution transfection on actual library screening efficacy, we chose as a test case to screen a library of mutants of the *Rp*BphP1 bacteriophytochrome (BphP)[21]. We mutated the PAS-GAF domains at amino acid positions 201, 202, 257 and 282 to NNS (N, any nucleotide; S, either T or C), based on previous studies on enabling fluorescence in BphPs[22]. The resulted site-directed library was transfected into HEK293T cells, the cells exhibiting fluorescence upon excitation with 640 nm laser were FACS sorted (reducing the cell count from ~50M to ~60k), and then robotically cell picked based upon brightness (reducing the cell count from ~25-35k to 45). To evaluate the *Rp*BphP1 mutants expressed in the 45 picked cells, the genes recovered from the pool of extracted cells were cloned into expression vectors and 184 clones were randomly selected for further characterization. Only 85 out of 184 selected clones (all with unique nucleotide sequences, corrected for duplications) exhibited near-infrared fluorescence upon expression in HEK cells. To find out why over half of the clones were non-functional, all selected clones were sequenced. Sequence analysis revealed multiple point mutations scattered throughout the entire gene with on average ~2.3 nucleotide mutations per gene in addition to the intended mutations at amino acid positions 201, 202, 257 and 282. Only about 12% of recovered genes had no nucleotide mutations beyond those at these 4 intended sites, while about ~66% contained 1 to 3 nucleotide mutations at sites beyond the 4 intended sites. Panel **c** illustrates distribution of nucleotide mutation counts in the *Rp*BphP1 PAS-GAF domains recovered from HEK293T cells transfected with the gene library using our calcium phosphate transfection protocol. This data implies that HEK293T cells introduced $2.4 \cdot 10^{-3}$ nucleotide mutations per base pair of exogenous DNA. Indeed, HEK293T cells have been reported to mutate plasmids delivered by calcium phosphate transfection[23]. Note well: according to earlier studies the mutation count of exogenous DNA by such mammalian cells did not show a progressive rise over time, but rather was constant across the studied time course (6-96 h)[23,24]. These results suggested that the mutations were introduced soon after transfection, rather than continuously over time. Therefore, extended culturing of cells, e.g. over the time course of a screen, does not likely result in accumulation of undesired mutations during the extended trajectory of an experiment. This may account for the high fidelity of our screen, in the sense that clones we obtained in the final analysis, reflected the high qualities obtained in initial screening steps. To estimate the exact number of plasmids delivered per single positive cell, we focused on sequence analysis of the intended-mutation regions. We repeated the robot cell picking for the same gene library and extracted 8 cells that exhibited bright near-infrared fluorescence. Each of 8 extracted cells was placed into a separate PCR tube for gene recovery. For each cell, 24 colonies were selected randomly for further characterization. For 4 of the cells, all of the recovered clones had a single

common set of nucleotides at the 12 bases that were mutated intentionally, suggesting a single plasmid was transfected (although the 24 colonies yielded, due to the aforementioned HEK mutation effect, an average of 22 ± 1 (mean ± SD) different clones per cell). For the other 4 cells, the clones that emerged from each cell contained 3-4 unique sets of nucleotides at the intended-mutation codons, implying triple or quadruple transfection (the 24 colonies yielded 21 ± 2 unique clones per cell). Among the entire set of recovered genes, 41% exhibited any near-infrared fluorescence upon expression in HEK cells. Thus, the mutagenic activity of HEK293T cells can inactivate protein function. Also, since multiple plasmids end up in a given cell, perhaps 4-5 (or more) recovered genes should be phenotyped per extracted cell to ensure identification of positive clones. (**d**) The amount of each plasmid in each DNA mixture, comprising pEGFP-N1, pmCardinal-N1 and pUC19 plasmids, used for transfection per well of 24-well plate, for the ratios presented in (**a**).

Supplementary Figure 2. Workflow of robotic cell picking based upon microscopy-derived imaging parameters.

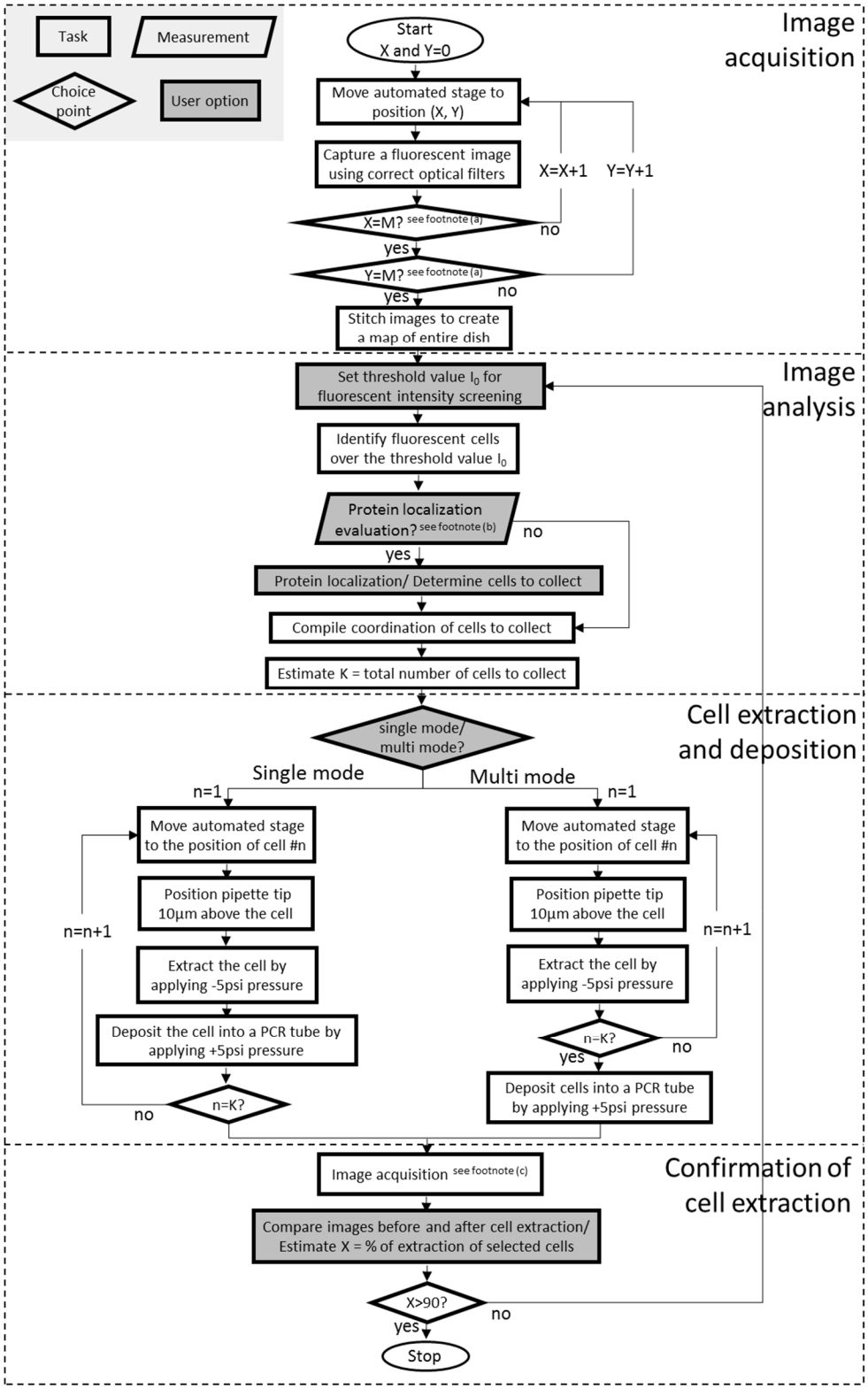

The cell picking process based upon microscopy-derived imaging parameters consists of image acquisition, image analysis, cell extraction and deposition using an automated micropipette, and confirmation of cell extraction. The CellSorter hardware[25] was installed on an inverted epi-fluorescent microscope (Nikon Eclipse T*i*) equipped with an automated stage (Ludl). "Single-mode" operation of the cell picker is used for isolation of a single cell per extraction-deposition cycle with the user-selectable option to collect extracted cells one per tube, and "multi-mode" operation is used for collection of multiple cells into a single tube. In this study, we used "single-mode" operation, but in principle, some screens might be amenable to a multi-mode strategy (which in principle can go faster because tube switching is not needed). (**a**) M was 12 when a 3 cm cell culture dish (Falcon) was imaged using a 10x objective lens and an sCMOS camera (Zyla 5.5, Andor). (**b**) Protein localization evaluation was performed on voltage sensor variants with brightness exceeding a threshold value I_0. In this study, the evaluation was manually conducted by examining whether voltage sensor fluorescent signals exclusively came from plasma membranes or not. Matlab code was developed to automate the protein localization evaluation by comparing fluorescent signals of membrane localized GFPs to those of protein(s) of interest. (**c**) Image acquisition was repeated in the same way as described in the first part of the flowchart.

Supplementary Figure 3. Directed molecular evolution of monomeric near-infrared FPs in HEK293T cells using FACS and robotic cell picking with microscopy image-based criteria.

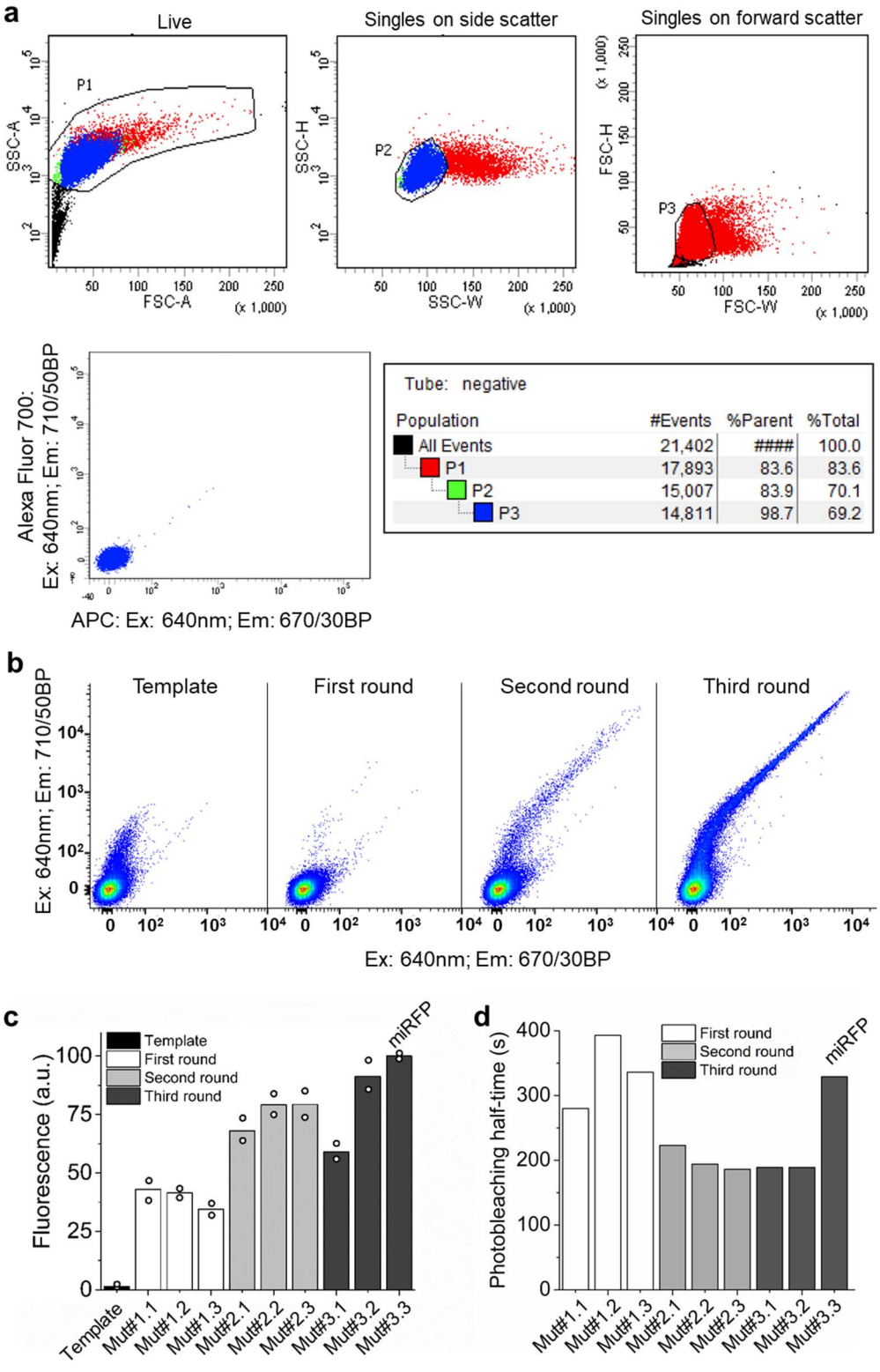

As a starting template for directed molecular evolution, we selected the *Rp*BphP1 bacteriophytochrome (BphP)[21], reasoning based on the crystal structure of *Rp*BphP1 (*ref* [26]) that this protein could serve as a viable backbone for engineering monomeric near-infrared FPs because of a lack of dimerization at its PAS-GAF domains (unique amongst bacteriophytochrome crystal structures). We performed three sequential rounds of directed molecular evolution using robotic cell-picking with microscopy image-based criteria to screen for the clones with improved brightness (see **Supplementary Table 3** for screening parameters). The number of positive cells, as well as the mean fluorescence intensity of positive cells in the generated random libraries, increased in each round of directed molecular evolution. Panel **a** illustrates gating strategy applied throughout this paper to sort singlets of live cells using flow cytometry. First, debris and dead cells were gated out using forward and side scatter area (FCS-A and SSC-A; *upper left FACS dot-plot*), and then cell aggregates were gated out using side and forward scatter width and height (SSC-W, SSC-H, FSC-W, FSC-H; *upper middle and right FACS dot-plots*) before desired fluorescence channels were used to analyze cells (*lower left FACS dot-plot*). Example of numerical values for numbers and percentages of cells are shown in the table (*lower right table*). (**b**) FACS dot-plots representing near-infrared fluorescence of HEK293T cells expressing the *Rp*BphP1 PAS-GAF template ("Template") and gene libraries generated in the first, second and third rounds of directed molecular evolution (see **Supplementary Table 3** for details). (**c**) The brightness of the top three clones selected in each round also increased throughout directed molecular evolution. Mean near-infrared fluorescence intensity of HEK293T cells expressing template protein (*black bar*) and individual clones selected in the first (*open bar*), second (*gray bar*) and third (*dark gray bar*) rounds of directed molecular evolution (open circles, data points; n = 2 transfected samples from the same passage culture each). Compared to the template, the mutants found in the first round had various combinations of the N19D; A28V; D72G; R97C; S102P; A149D; F181Y; D201V,M,L; I202V; D241Y; I253T; Y257F,M; M261L; and A282I,V substitutions. Compared to the template, the mutants found in the second round had various combinations of the A11D; L17P; N19D; D72G; V92T; R97C; A149V,D; F181Y; R184I; D201V,L; I202V; D241H,Y; Y257F; M261L; and A282I,V,C substitutions. Compared to the template, the mutants found in third round had various combinations of the A11D; L17P; N19D; A36T; D44G; A93T; A149V; F181Y; R184I; D201V,L; I202V; I253T; Y257F; and A282I,V substitutions. The Mut#3.3 clone was named miRFP and selected for further characterization. Open circles, data points. Imaging conditions are the same as in **Supplementary Fig. 4b**. (**d**) Mean photobleaching half-time of individual clones selected in the first (*open bar*), second (*grey bar*) and third (*dark grey bar*) rounds of directed molecular evolution measured in live HEK293T cells, measured for one field of view containing 3-5 cells per construct (shown are raw data, not normalized for photonic dosage). Imaging conditions are the same as in **Supplementary Fig. 4d**. These data indicate that our developed methods for expression and screening of large gene libraries in mammalian cells as well as genotyping of selected cells can be efficiently used for directed molecular evolution and sensitive enough even for developing brightly fluorescent proteins from a non-fluorescent template.

Supplementary Figure 4. Characterization of miRFP *in vitro* and in cultured cells.

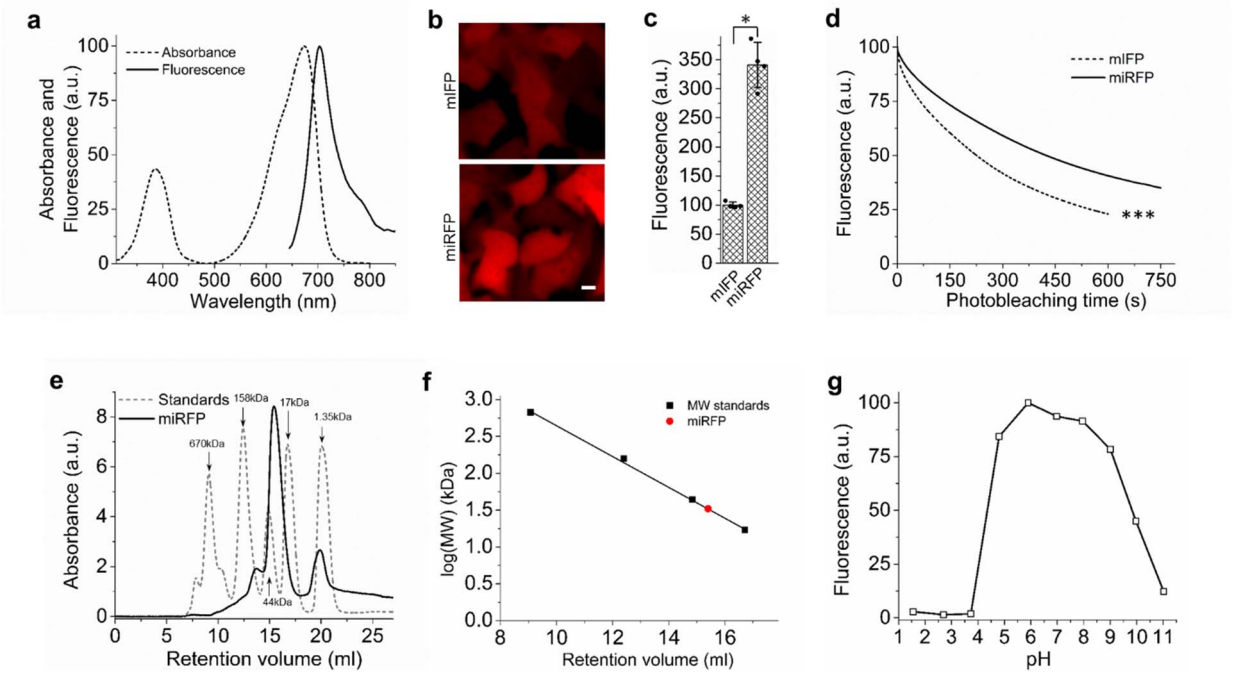

(**a**) Absorbance (dotted line) and fluorescence (solid line) spectra of miRFP. (**b**) Representative fluorescence images of HEK293T cells expressing mIFP and miRFP (n = 4 fields of view from two independent transfections from the same culture passage). Scale bar: 10μm. Excitation (λ_{ex}) 628/31BP (bandpass, used throughout; all wavelength numbers are in nm) from a LED at 62 mW/mm^2 and emission (λ_{em}) 664LP (longpass, used throughout) used for (**b, c, d**). (**c**) Mean fluorescence intensity of HEK293T cells transfected with mIFP and miRFP encoding plasmids (n = 4 fields of view from two independent transfections from the same culture passage; individual data points in black dots; **P* = 0.0286, Wilcoxon rank sum test; see **Supplementary Table 5** for full statistics). Back dots, individual data points; vertical bars, mean; error bars, standard deviation. (**d**) Photobleaching curves of mIFP and miRFP expressed in HEK293FT cells (n = 8 cells from 1 transfected sample, each; ****P* = 0.0001554, Wilcoxon rank sum test of photobleaching half times). (**e**) Size-exclusion chromatography demonstrated that the mutant was 96% monomeric at a high concentration. Size exclusion chromatography of miRFP at a concentration of 4 mg/ml (*solid line*), and indicated molecular weight (MW) standards (*dashed line*). Apparent molecular weight of miRFP was ~33.6 kDa calculated at its major peak, and ~75.8 kDa calculated at its minor peak. The ratio of dimer to sum of dimer and monomer, estimated as the ratio of corresponding peak areas, was ~4% (n = 1 technical replicate). (**f**) Size exclusion chromatography calibration plot showing the relative retention volumes of protein molecular weight standards (*black squares*; Gel Filtration Standard, Bio-Rad; n = 1 technical replicate) and miRFP at its major peak (*red circle*). (**g**) The fluorescence of miRFP was stable at pH 5-9 with a pKa value of 4.3. Plotted is equilibrium pH dependence of miRFP fluorescence (n = 3 technical replicates).

Supplementary Figure 5. Alignment of amino acid sequences of the *Rp*BPhP1 PAS-GAF domains and miRFP.

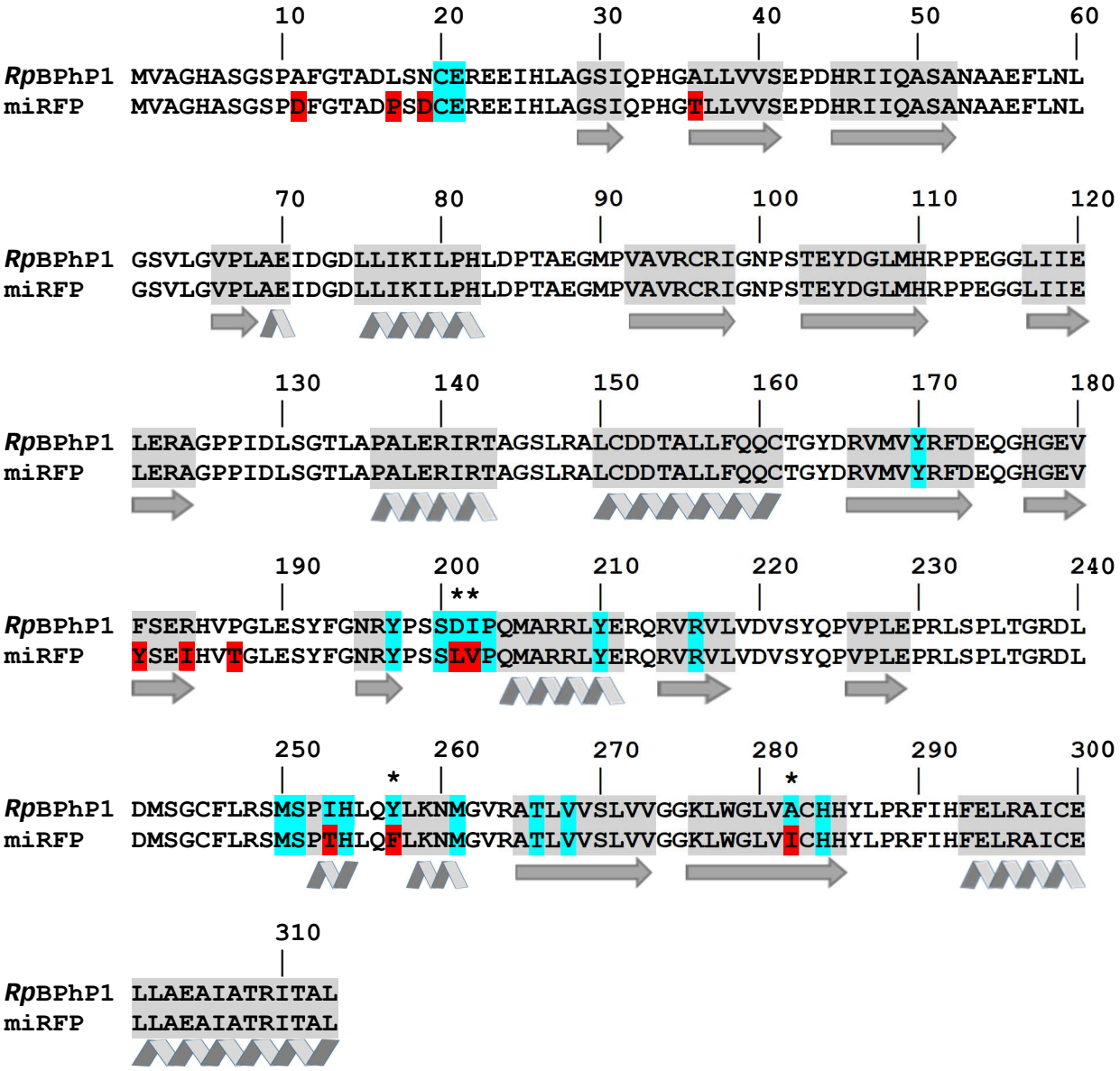

The residues surrounding the chromophore (within 4.0 Å) are highlighted in cyan. Mutations resulting in the conversion of parental *Rp*BphP1 into the miRFP variant are highlighted in red. The β-sheet-forming regions and α-helixes are shaded and denoted with arrows and ribbons, respectively. Amino acid positions selected for site-directed mutagenesis are marked with asterisks.

Supplementary Figure 6. Wide-field fluorescence imaging of miRFP fusion proteins in live HeLa cells.

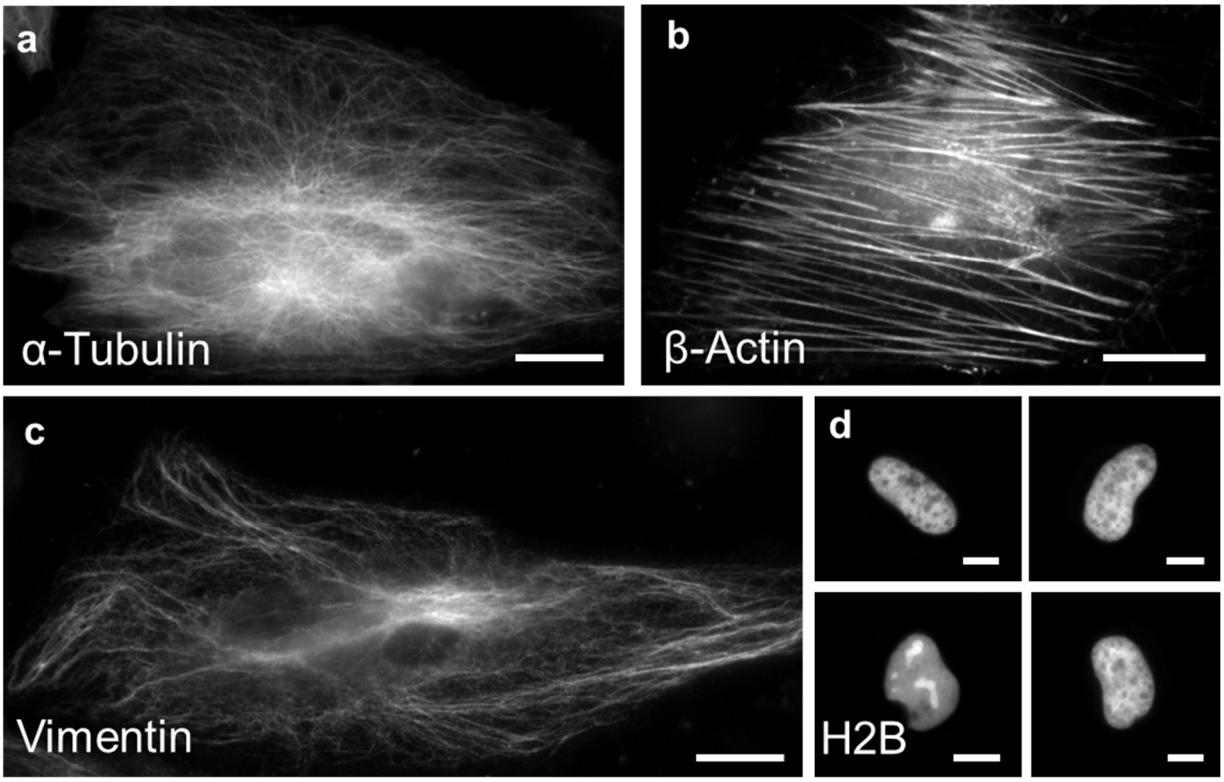

The miRFP fusions to α-tubulin, β-actin, vimentin and H2B (as used in *ref.* [27]) localized properly in live mammalian cells, demonstrating its usefulness as a monomeric fusion tag. Representative wide-field fluorescence images of live HeLa cells transfected with (**a**) miRFP-α-Tubulin (n = 25 cells from two independent transfections), (**b**) miRFP-β-Actin (n = 15 cells from two independent transfections), (**c**) miRFP-Vimentin (n = 11 cells from two independent transfections, and (**d**) miRFP-Histone 2B (H2B; n = 17 cells from two independent transfections). Scale bars, 10 μm.

Supplementary Figure 7. Expression of miRFP in primary cultured mouse hippocampal neurons, mouse brain and zebrafish larvae and characterization of two-photon properties of miRFP.

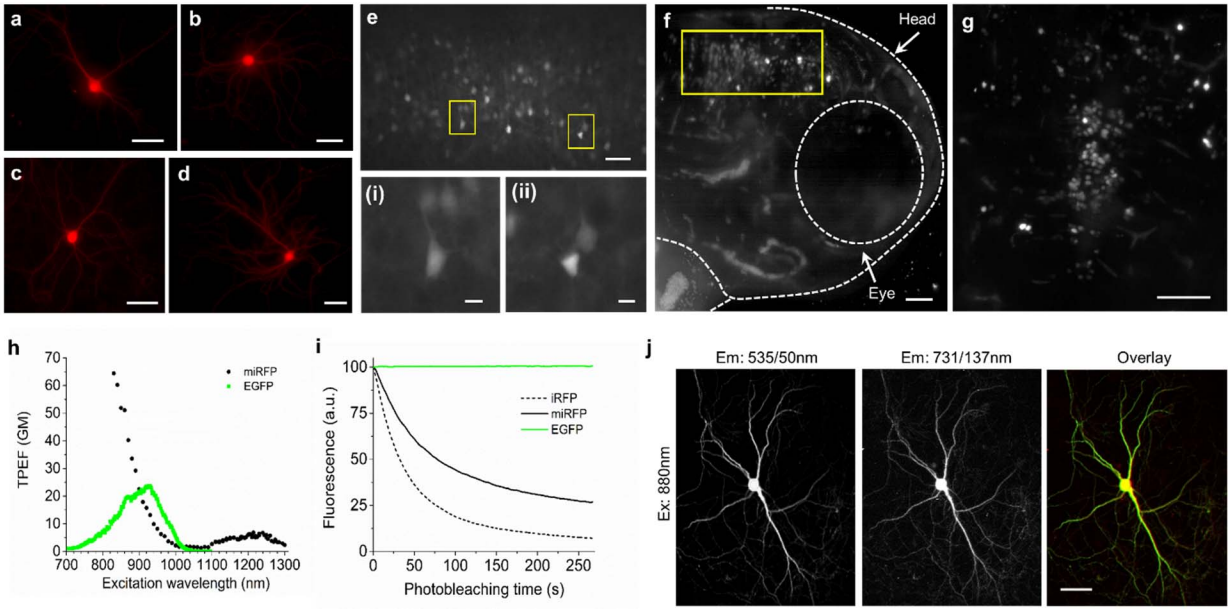

When expressed without heme oxygenase-1, which is required to enable mIFP fluorescence *in vivo*[12], miRFP functioned well in cultured neurons, zebrafish larvae, and mouse brain, and even could be co-excited with EGFP via two photon excitation using a standard Ti-Sapphire laser. (**a-d**) Representative fluorescence images of primary cultured mouse hippocampal neurons expressing miRFP at (**a**, **b**) 15 and (**c**, **d**) 24 days *in vitro* (DIV; n = 20 neurons from 2 cultures). Scale bars, 50 μm. (**e**) Representative fluorescence images of coronal sections of mouse brain with neurons expressing miRFP under Syn promoter (n = 8 slices from 2 mice). Scale bar, 50 μm. (**i, ii**) Magnified views of the neurons in the boxed regions of (**e**). Scale bars, 10 μm. Expression of miRFP was targeted by *in utero* electroporation (IUE; embryonic day (E) 15.5). (**f-g**) Overview of transient expression of miRFP in zebrafish larvae (n = 10 fish from two independent injections). miRFP was expressed in zebrafish larvae without co-injection of heme oxygenase-1 mRNA. (**f**) Representative image of a lateral view of the brain of a zebrafish larva at 4dpf imaged on a light sheet microscope (Zeiss Lightsheet Z.1). (**g**) Magnified top view of the brain area selected in the yellow box shown in (**f**). Scale bars, 50 μm. (**h**) Two-photon excited fluorescence (TPEF) measured for miRFP (*black circles*) and EGFP (*green circles*). TPEF of miRFP was similar to that of dimeric iRFPs[28]. GM, Goeppert-Mayer units. (**i**) Raw photobleaching curves for iRFP (n= 9 neurons from 2 cultures; dashed line), miRFP (n = 6 neurons from 2 cultures; solid black line) and EGFP (n = 6 neurons from 2 cultures; green solid line) expressed in live cultured primary mouse neurons measured under two-photon excitation at 880 nm and 4.05 mW of total power. (**j**) Representative two-photon fluorescence images of cultured neurons co-expressing EGFP (*left*) and miRFP (*middle*) under 880 nm excitation (*right*, overlay, with EGFP in green and miRFP in red; n = 5 neurons from one culture). Scale bar, 10 μm.

Supplementary Figure 8. Screening workflow for simultaneous multiparameter optimization of genetically encoded voltage sensors.

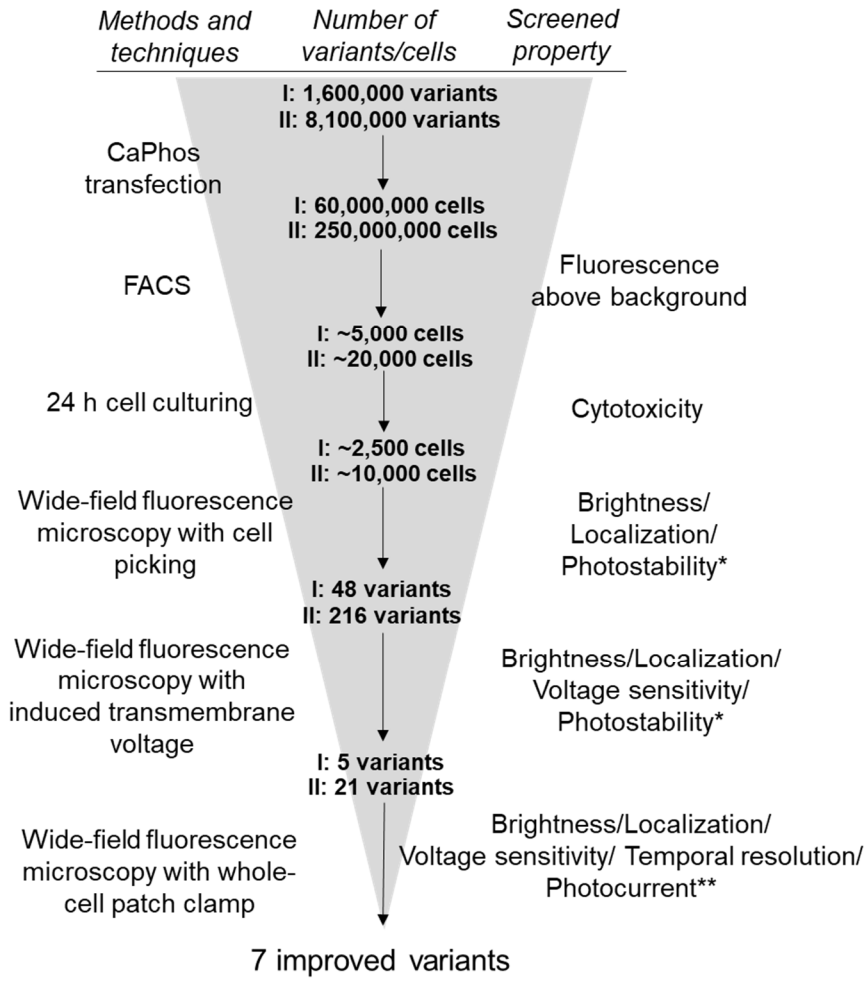

Screening workflow for simultaneous multiparameter optimization to develop a voltage sensitive fluorescent protein. *, photostability was tested on only 1/10th of the selected cells, and then discontinued since photobleaching was universally slow (i.e., good). **, photocurrent was tested on 4 out of 21 variants in the final round. CaPhos, calcium phosphate transfection. Roman numerals I and II indicate the first and second passes through the pipeline, respectively.

Supplementary Figure 9. Alignment of amino acid sequences of Archaerhodopsin-2 (aR2), Archaerhodopsin-3 (Arch), Archer1, Arch-7, QuasAr1, QuasAr2 and voltage sensor variants selected in the first round of directed molecular evolution.

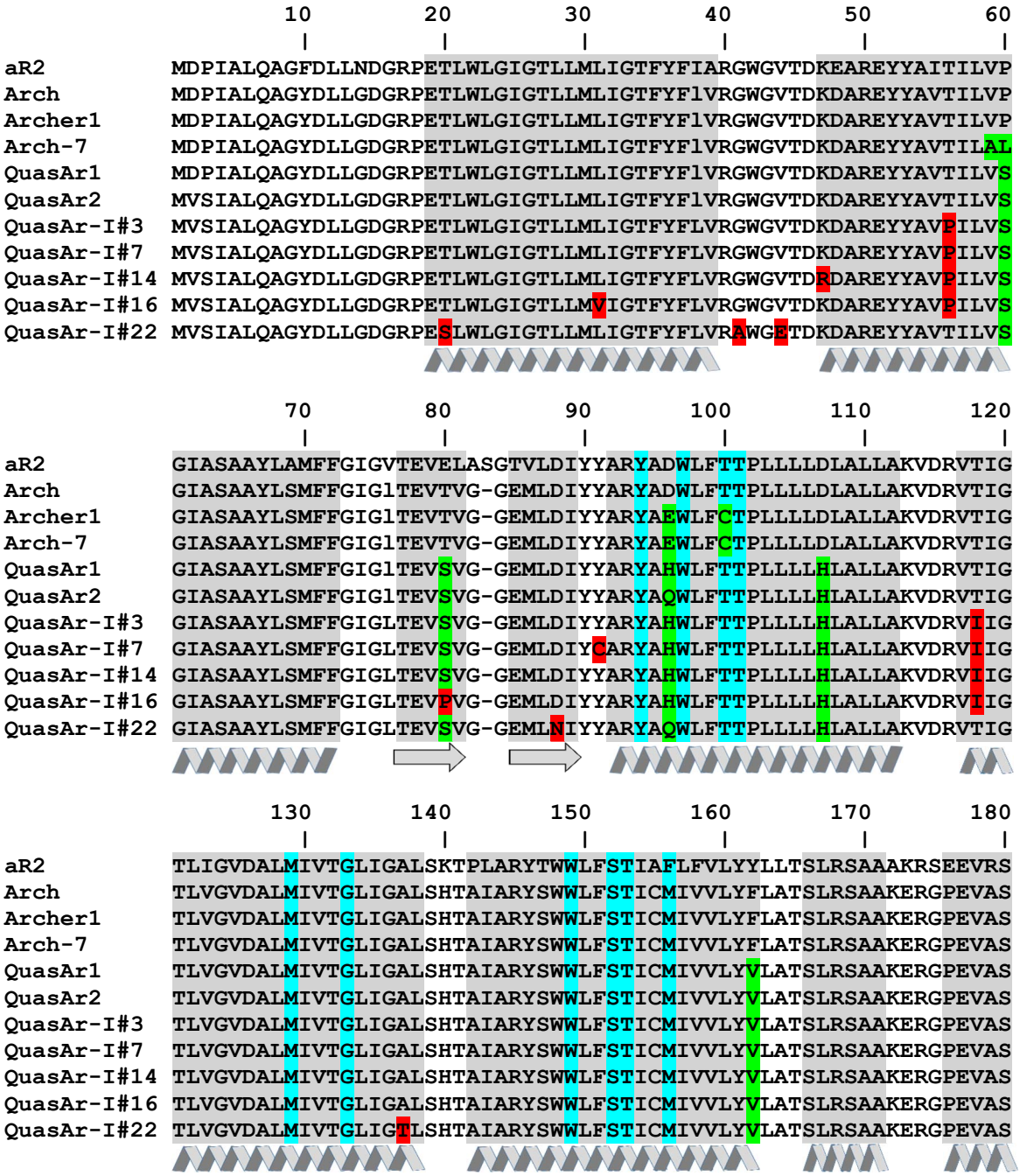

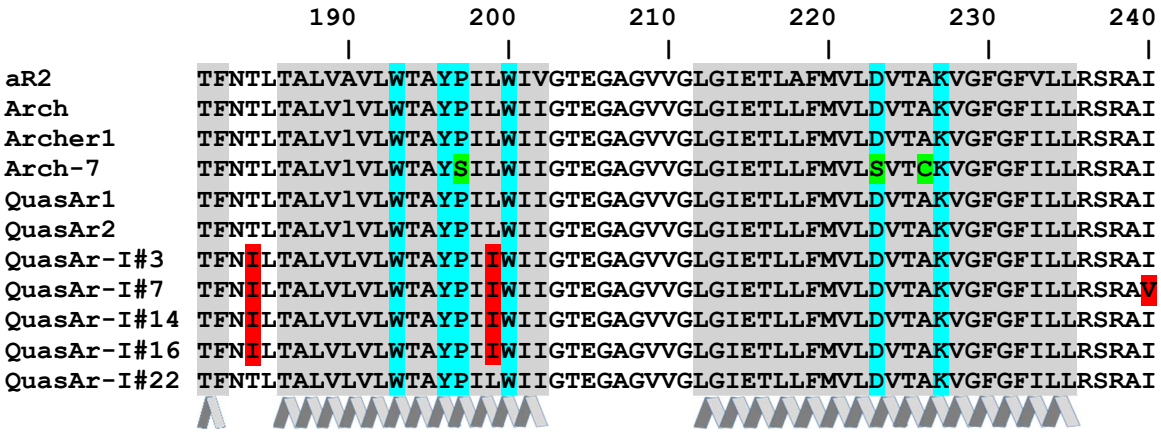

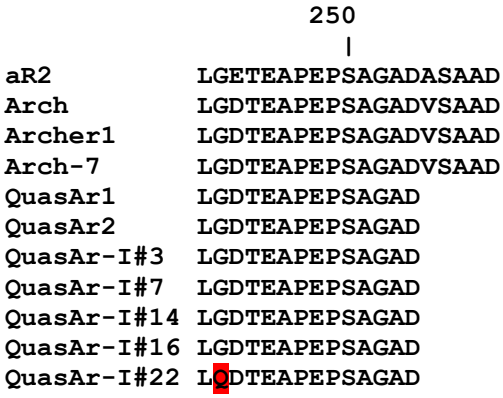

Amino acid numbering follows that of aR2. The chromophore-surrounding residues (within 4.0 Å) are highlighted in cyan. Mutations resulting in the conversion of the parental Arch into Archer1, Arch-7, QuasAr1, and QuasAr2 variants are highlighted in green. Mutations introduced during the first round of directed molecular evolution are highlighted in red. The β-sheet-forming regions and α-helixes are shaded and denoted with arrows and ribbons, respectively.

Supplementary Figure 10. Screening and characterization of selected Archon variants in comparison to their parental protein in HEK293T cells.

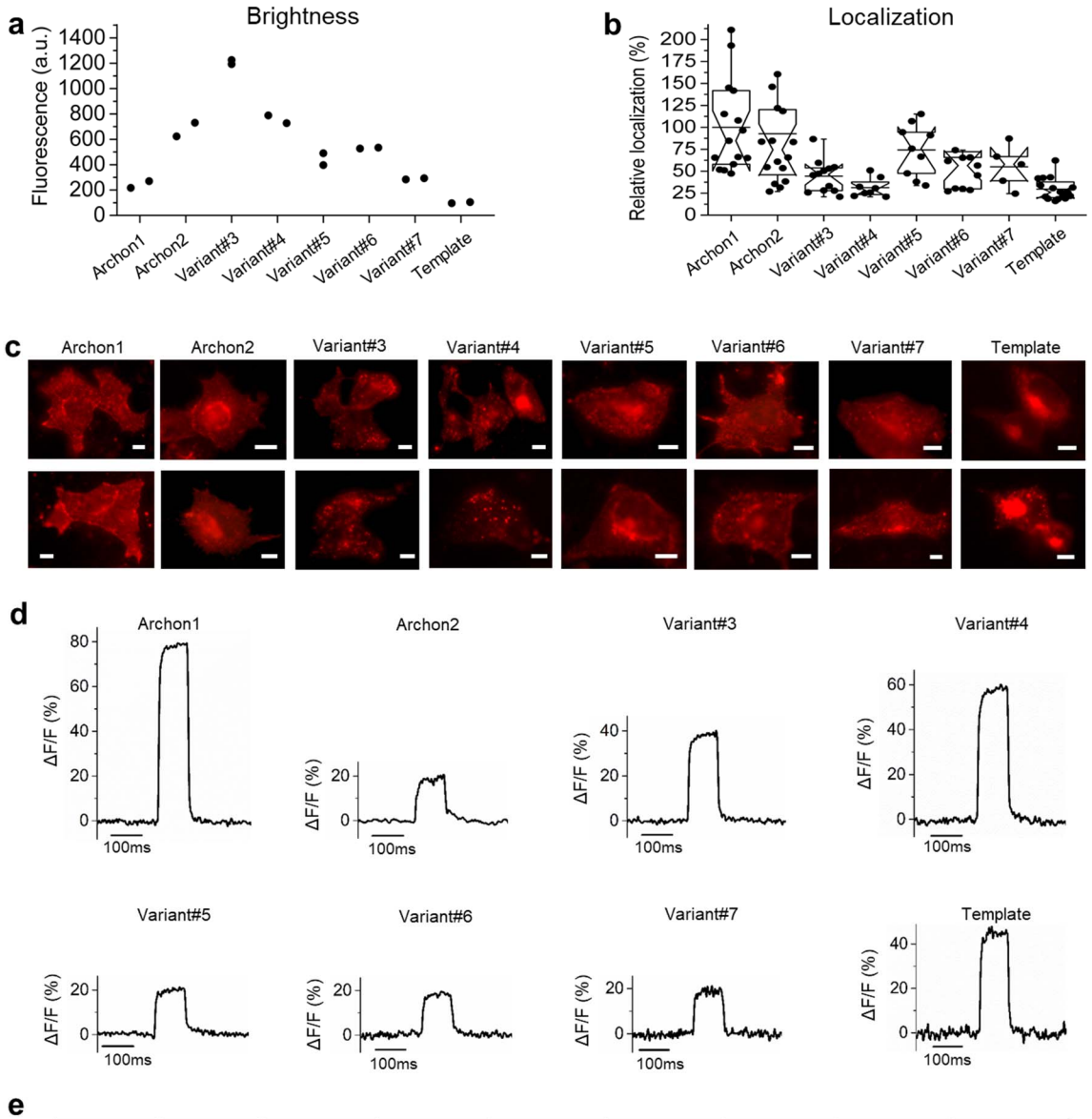

Kinetics, ms	Archon1	Archon2	Variant#3	Variant#4	Variant#5	Variant#6	Variant#7	Template
τ_{on}	3.6	2.6	5.3	4.0	2.6	3.5	3.7	2.3
τ_{off}	1.7	4.0	13	5.0	5.2	4.2	3.2	0.6

(**a**) Relative fluorescence brightness of selected Archon variants compared to the template (fluorescence brightness was measured using flow cytometry as in **Fig. 1e,** 2 independent transfections per construct were used for flow cytometry analysis; transfection, culturing, and FACS parameters including light power were the same across all indicators). Black dots, individual data points. (**b**) Relative membrane localization of Archon variants compared to the template. Membrane localization analysis and imaging conditions were the same as in **Fig. 1d** (n = 15, 16,

12, 8, 9, 11, 5, 16 cells for Archon1, Archon2, Variant#3, Variant#4, Variant#5, Variant#6, Variant#7, and the template, from one culture each, respectively). Box plots with notches are used (see caption for **Fig. 1d** for description). Black dots, individual data points. (**c**) Representative fluorescence images of HEK293T cells expressing Archon variants. Imaging conditions same as in **Fig. 1c** (n = 15, 16, 12, 8, 9, 11, 5, 16 cells for Archon1, Archon2, Variant#3, Variant#4, Variant#5, Variant#6, Variant#7, and the template, from one culture each, respectively). Dynamic range for all images was normalized to facilitate visual comparison of membrane localization across selected variants (see panel **a** for fluorescence brightness quantification). Scale bar, 5 μm. (**d**) Representative fluorescence traces of Archon variants in response to 100 mV changes in membrane voltage (from -70 to +30 mV). Traces were recorded as in **Fig. 1f** (n = 6, 4, 9, 3, 7, 3, 3, 5 cells for Archon1, Archon2, Variant#3, Variant#4, Variant#5, Variant#6, Variant#7, and the template, from two cultures each, respectively). (**e**) Kinetics of on and off responses for Archon variants vs. template during 100 mV voltage steps (from -70 to +30 mV; n = 6, 4, 9, 3, 7, 3, 3, 5 cells for Archon1, Archon2, Variant#3, Variant#4, Variant#5, Variant#6, Variant#7, and the template, from two cultures each, respectively). τ_{on} and τ_{off} are defined as the duration between the onset of the fluorescence rise and fall, respectively, and the time the fluorescence reaches half of the final amplitude. The values are calculated by a custom script in MATLAB.

Supplementary Figure 11. Alignment of amino acid sequences of Archaerhodopsin-2 (aR2), Archaerhodopsin-3 (Arch), Archer1, QuasAr1, QuasAr2 and voltage sensor variants selected in the second round of directed molecular evolution.

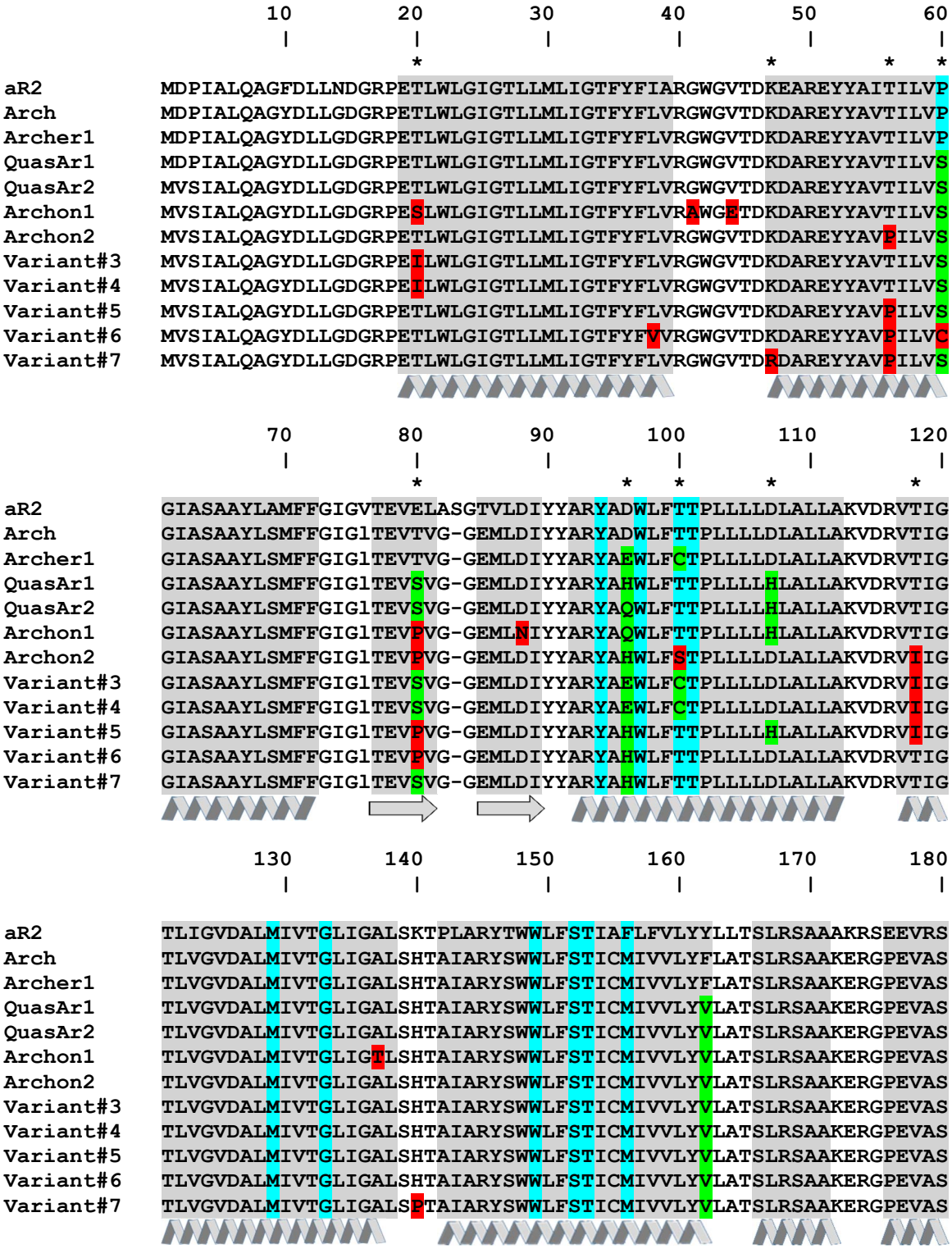

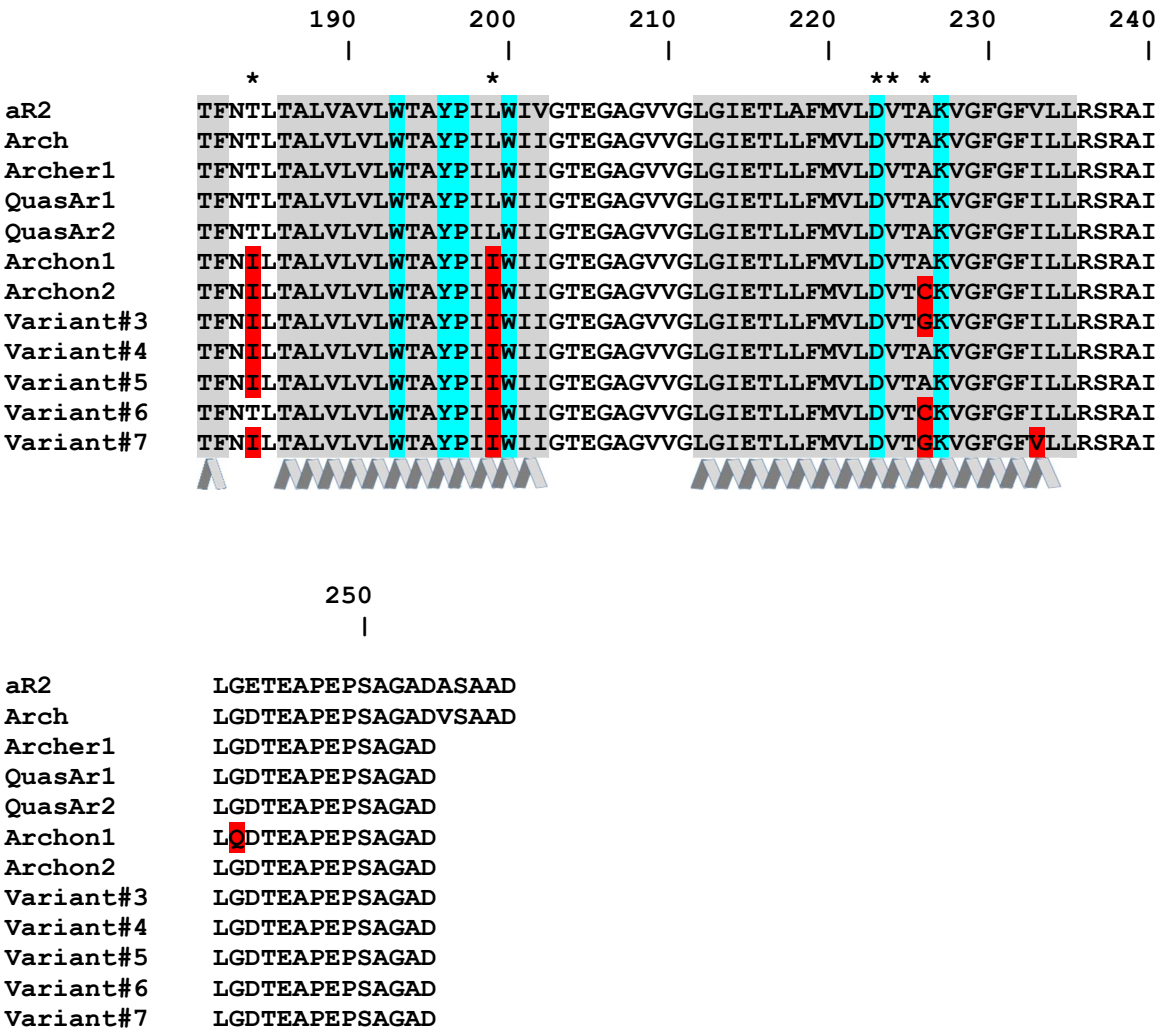

Amino acid numbering follows that of aR2. The chromophore-surrounding residues (within 4.0 Å) are highlighted in cyan. Mutations resulting in the conversion of the parental Arch into Archer1, Arch-7, QuasAr1, and QuasAr2 variants are highlighted in green. Mutations introduced during the first round of directed molecular evolution are highlighted in red. The β-sheet-forming regions and α-helixes are shaded and denoted with arrows and ribbons, respectively. Amino acid positions selected for site-directed mutagenesis are marked with asterisks.

Supplementary Figure 12. Images of cultured primary mouse hippocampal neurons expressing Archon1 fusions.

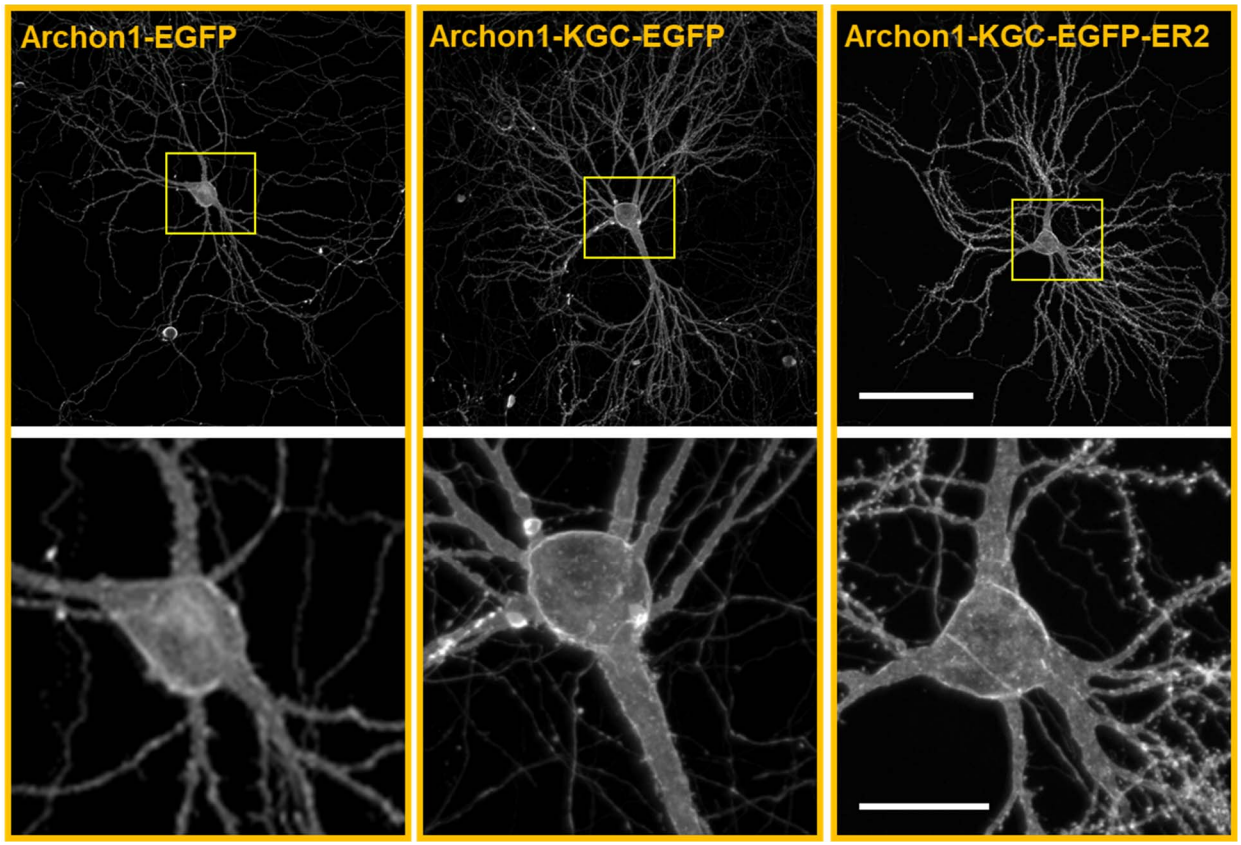

(*Top*) Representative confocal images of cultured mouse hippocampal neurons (17 days in vitro (DIV)) expressing Archon1-EGFP, Archon1-KGC-EGFP, and Archon1-KGC-EGFP-ER2 (imaged via EGFP fluorescence using laser excitation at λ_{ex}= 488 nm and λ_{em}= 525/50BP; n = 10, 10 and 32 neurons from 1, 1 and 5 cultures, respectively). In this figure panel only, we use Archon1 to refer to the bare opsin without trafficking sequences; for convenience, in the rest of the paper we simply refer to Archon1-KGC-EGFP-ER2 as Archon1-EGFP for short, since we always use it with KGC and ER2 trafficking sequences elsewhere. The yellow boxes in the top panels indicate regions shown below at higher magnification. Scale bar, 100μm. (*Bottom*) High magnification images of the neurons highlighted in yellow boxes in the top panels. Scale bar, 25 μm.

Supplementary Figure 13. Images of cultured primary mouse hippocampal neurons expressing selected voltage sensors.

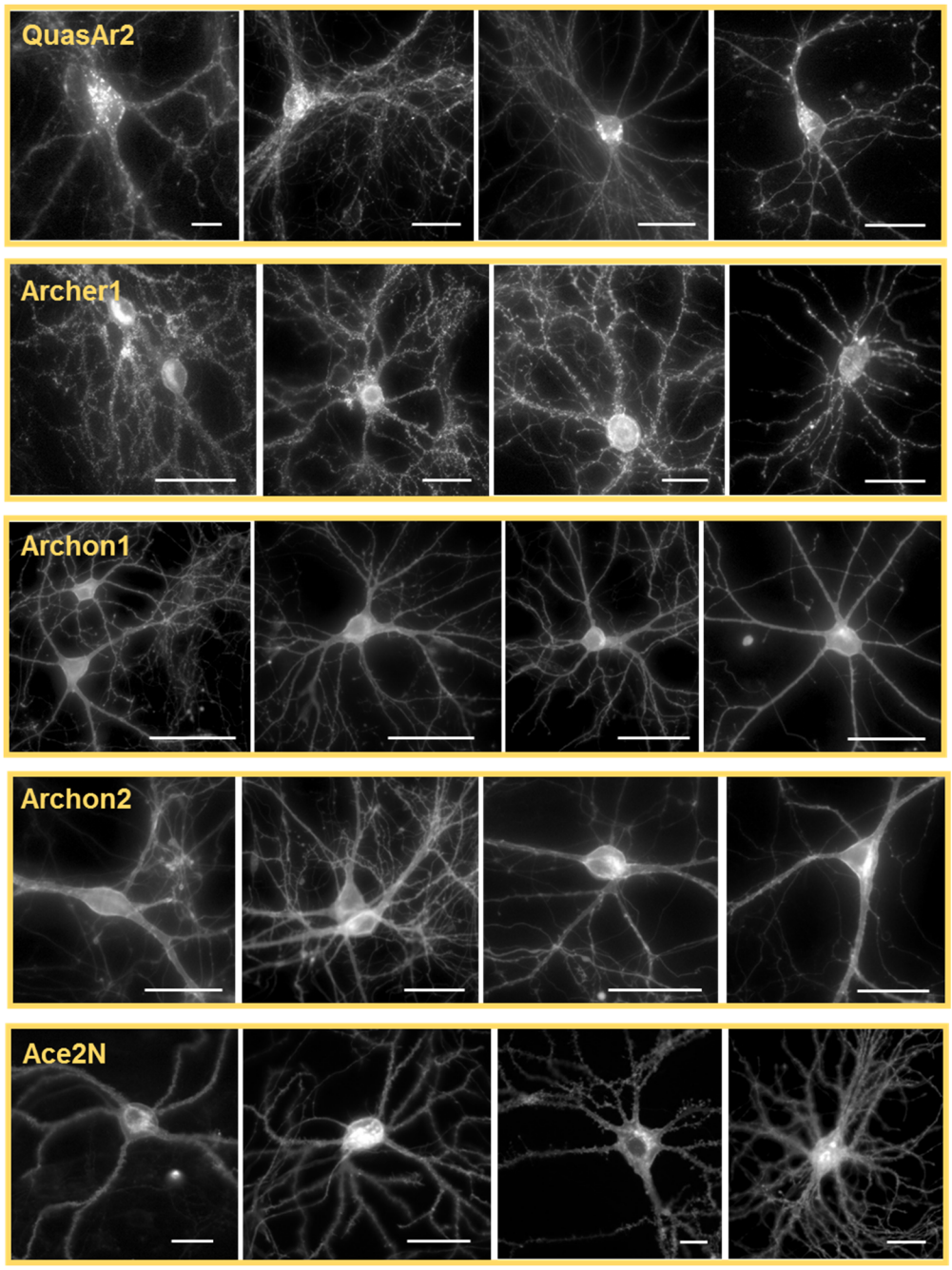

Representative images of cultured mouse hippocampal neurons (12-15 DIV) expressing QuasAr2-mOrange-KGC-ER2 (imaged via mOrange2 fluorescence: λ_{ex} = 586/20BP from an LED and λ_{em} = 628/32BP); Archer1-KGC-EGFP-ER2, Archon1-KGC-EGFP-ER2, Archon2-KGC-EGFP-ER2 (the last three were imaged via EGFP fluorescence using λ_{ex} = 474/23BP from an LED and λ_{em} = 527/50BP); Ace2N-4aa-mNeonGreen-KGC-ER2 (imaged via mNeonGreen fluorescence using λ_{ex} = 474/23BP from an LED and λ_{em} = 527/50BP; from the top; n = 18, 16, 32, 23, and 12 neurons from 4, 4, 5, 4, and 2 cultures, respectively). Scale bars, 20μm.

Supplementary Figure 14. Membrane properties of cultured primary mouse hippocampal neurons expressing selected voltage sensors.

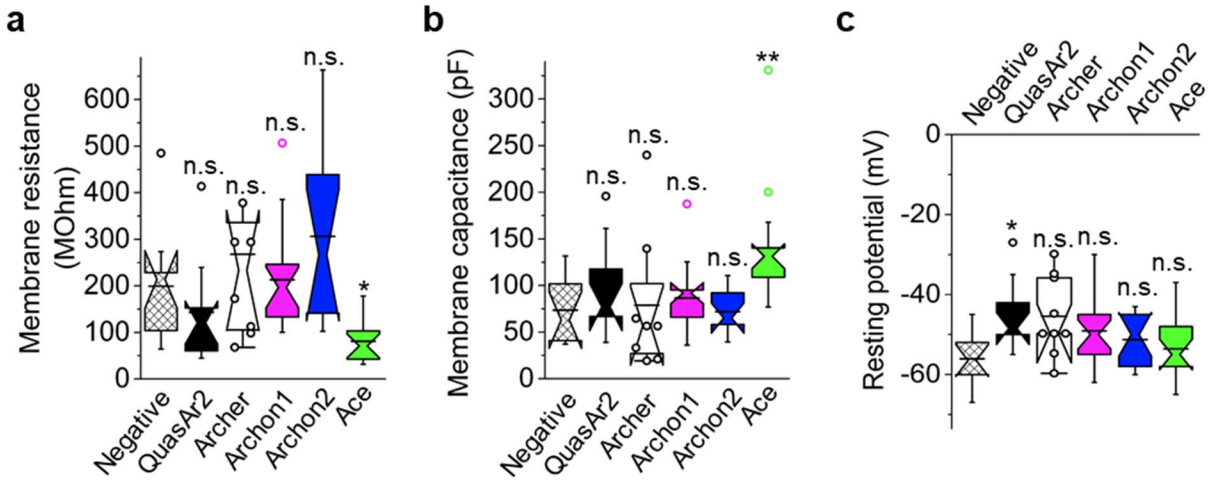

Cultured hippocampal neurons expressing QuasAr2 (n = 11 cells from two cultures), Archer1 (n = 9 cells from two cultures), Archon1 (n = 20 cells from four cultures), Archon2 (n = 14 cells from four cultures), and Ace2N-4aa-mNeon (Ace, n = 17 cells from one culture) were patched to compare membrane properties. Neurons were transfected by calcium phosphate transfection except the negative control (non-transfected neurons, n = 10 cells from two cultures). (**a**) Membrane resistance. $P > 0.05$, not significant (n.s.), throughout all panels of this figure; $*P = 0.0136$ compared to negative control; Kruskal–Wallis analysis followed by *post-hoc* Steel's test with negative as control group throughout this panel; see **Supplementary Table 5** for full statistics for **Supplementary Fig. 14**. (**b**) Membrane capacitance. $**P = 0.0077$ compared to negative control. (**c**) Resting potential. $*P = 0.0483$ compared to negative control. Throughout this figure, box plots with notches are used; narrow part of notch, median; top and bottom of the notch, 95% confidence interval for the median; top and bottom horizontal lines, 25% and 75% percentiles for the data; whiskers extend 1.5 times the interquartile range from the 25th and 75th percentiles; horizontal line, mean. For datasets with n < 10, open circles represent individual data points; data points which are less than the 25th percentile or greater than the 75th percentile by more than 1.5 times the interquartile range are also represented as open circles.

Supplementary Figure 15. Characterization of Archon1 in cultured primary mouse hippocampal neurons.

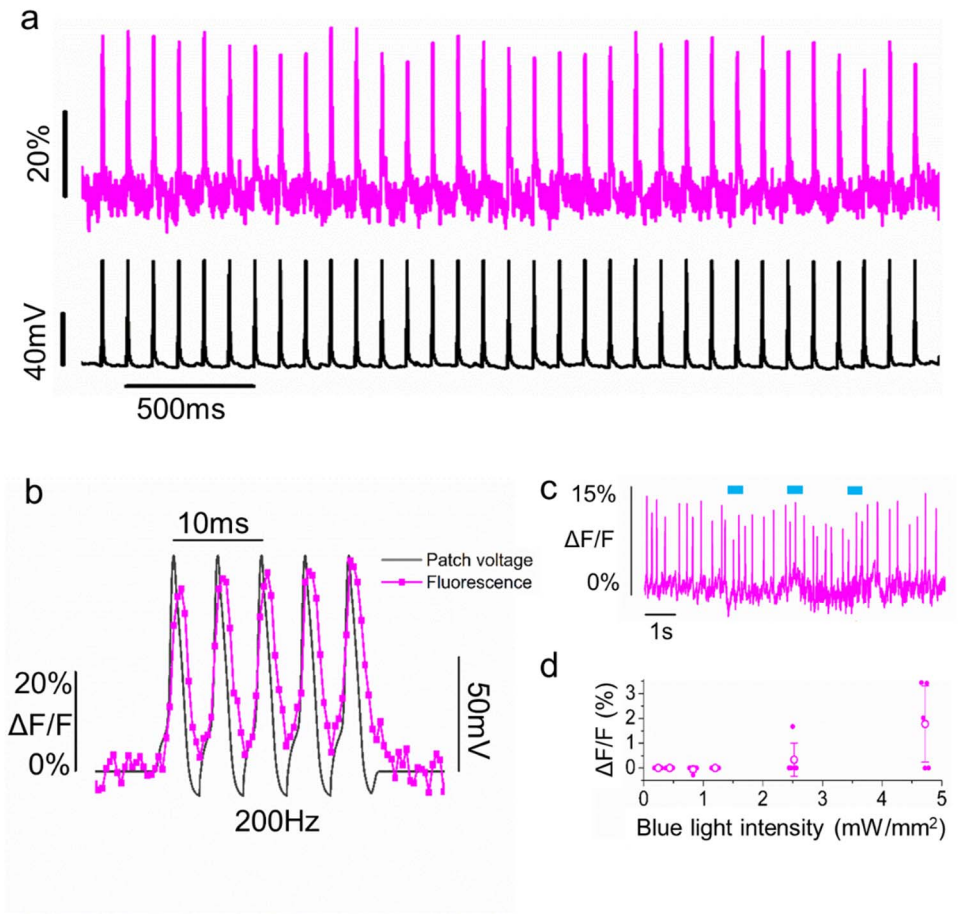

Characterization of Archon1 in cultured hippocampal neurons. (**a**) Representative single-trial optical recording of Archon1 fluorescence responses (magenta) to a 10 Hz action potential train evoked by current injections (400 pA, 5 ms); patch voltage is shown in black (λ_{ex} = 637 nm laser light at 800 mW/mm^2 and λ_{em} = 664LP, image acquisition rate: 2.3 kHz; n = 3 neurons from 2 cultures). (**b**) Representative single-trial optical recording of Archon1 fluorescence response to a 200 Hz action potential-like voltage transient train (black) in a voltage-clamped neuron (λ_{ex} = 637 nm laser light at 800 mW/mm^2 and λ_{em} = 664LP, image acquisition rate: 2.3 kHz; n = 3 neurons from 2 cultures). (**c**) Representative fluorescence trace of Archon1 in a spiking neuron during blue illumination (blue illumination: 470/20 nm light from an LED, 500 ms, 0.5 Hz, at 4.8 mW/mm^2; red illumination: 637 nm laser light at 800 mW/mm^2, λ_{em} = 664LP, image acquisition rate: 200 Hz; n = 5 neurons from one culture). (**d**) Optical crosstalk of blue illumination into Archon1 fluorescence measured in cultured neurons expressing Archon1 (n = 5 neurons from one culture), as in **c** (3-5 pulses for each illumination power), while holding red light power constant (as in **c**). Magenta open circles, mean; magenta dots, data points; error bars, standard deviation.

Supplementary Figure 16. Characterization of Archon2 in cultured primary mouse hippocampal neurons.

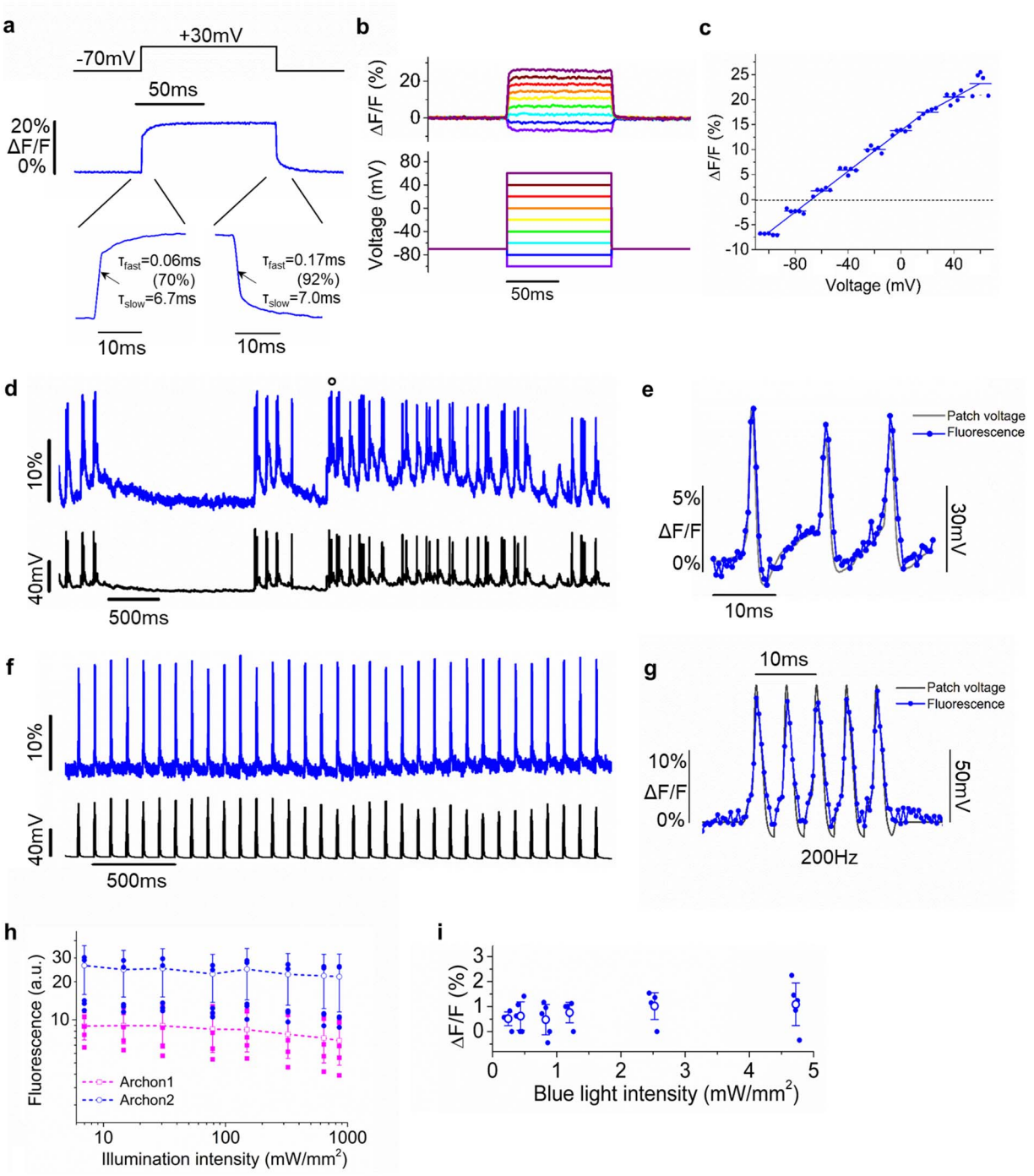

(**a**) A representative fluorescence response of Archon2 in a cultured neuron, to a 100mV change delivered in voltage-clamp. For panels **a-g** the imaging conditions were the following: excitation (λ_{ex}) at 637nm laser light, 800mW/mm^2, emission (λ_{em}) at 664LP, and image acquisition rate: 3.2 kHz. Archon2 exhibited 19 ± 2% of ΔF/F (mean ± standard deviation; n = 9 cells from 4 cultures) for a 100 mV deflection. τ_{fast} and τ_{slow} indicate time constants with the fluorescence trace fit

according to $\frac{\Delta F}{F}(t) = Ae^{-t/\tau fast} + Be^{-t/\tau slow}$, with the % indicating A/(A+B) (n = 8 neurons from 2 cultures). (**b**) Representative fluorescence traces of Archon2 in response to a series of voltage steps in voltage-clamp mode. Image acquisition rate: 2.3 kHz. (**c**) Population data corresponding to the experiment of **b** (n = 5 neurons from 3 cultures). (**d**) Representative single-trial optical recording of Archon2 fluorescence responses (*blue*) during spontaneous activity, and patching in current clamp (*black*) in a cultured hippocampal neuron (n = 3 neurons from two cultures). Peaks marked with circle (○) are zoomed-in in (**e**). Image acquisition rate: 2.3 kHz. (**e**) Zoomed-in view of peaks marked with circle (○) in (**d**). (**f**) Representative single-trial optical recording of Archon2 fluorescence responses (*blue*) to a 10Hz action potential train evoked by current injections (400 pA, 5 ms); patch voltage is shown in black (n = 2 neurons from one culture). Image acquisition rate: 2.3 kHz. (**g**) Representative single-trial optical recording of Archon2 fluorescence response to a 200 Hz action potential-like voltage transient train (*black*) in a voltage-clamped neuron (n = 3 neurons from two cultures). Image acquisition rate: 2.3 kHz. (**h**) Fluorescence of Archon1 (*magenta*) and Archon2 (*blue*) as a function of illumination (n= 5 neurons from one culture, each). λ_{ex} = 637 nm laser light, λ_{em}= 664LP. Dots, individual data points; open symbols, mean; error bars: standard deviation. (**i**) Optical crosstalk of blue illumination into Archon2 fluorescence measured in cultured neurons expressing Archon2 (n = 5 neurons from one culture), as in **Supplementary Fig. 15c** (3-5 pulses for each illumination power). Blue dots, individual data points; blue open circles, mean; error bars, standard deviation.

Supplementary Figure 17. Photocurrent measurements for Archon1, Archon2, Archer, QuasAr2, and Arch in HEK293FT cells.

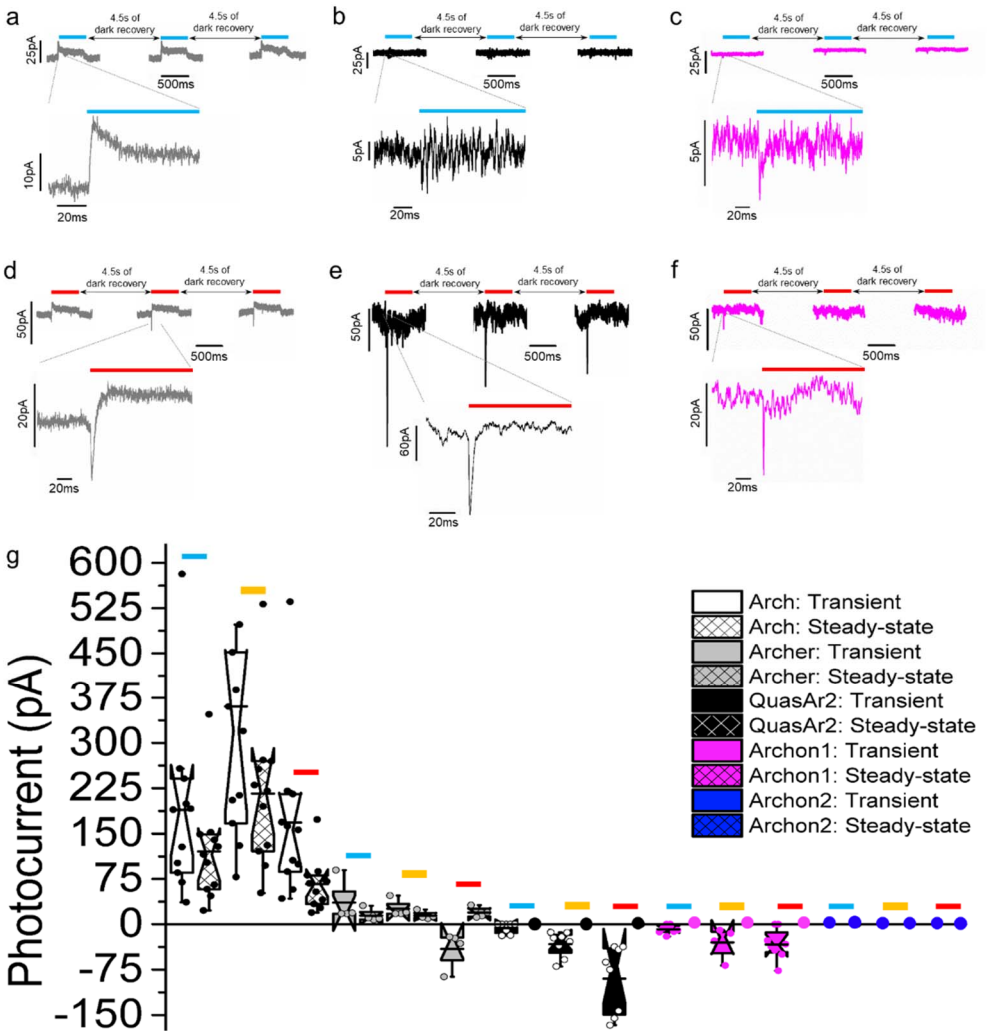

Representative traces (*top*) of (**a**) Archer, (**b**) QuasAr2, and (**c**) Archon1 photocurrent measured in HEK293FT cells in response to 470/20BP illumination from a blue LED (15 mW/mm^2, *blue bars*). Three pulses of blue light were applied with 4.5 second-long dark recovery periods. (*Bottom*) Zoomed-in views of the peaks of transient photocurrent of the top traces (n = 4, 8, and 8 cells from one, one, and two cultures for Archer, QuasAr2, and Archon1, respectively. (**d**, **e**, **f**) As in **a**, **b**, **c**, respectively, but with 637 nm laser illumination (800 mW/mm^2, *red bars*; n = 4, 8, and 8 from one, one, and two cultures for Archer, QuasAr2, and Archon1, respectively). (**g**) Population data for transient (*open columns*) and steady-state (*crosshatched columns*) photocurrents in response to 470/20BP light from an LED (15 mW/mm^2, *blue bars;* n = 11, 4, 8, 8, 4 cells from one, one, two, two, and one cultures for Arch, Archer, QuasAr2, Archon1, and Archon2, respectively), 550/20BP light from an LED (26 mW/mm^2, *orange bars*; n = 11, 4, 8, 4, 4 cells from one, one, two, one, and one cultures for Arch, Archer, QuasAr2, Archon1, and Archon2, respectively), 631/28BP light from an LED (24 mW/mm^2, *red bar*; n = 11 cells from one culture for Arch) and 637 nm laser light (800 mW/mm^2, *red bars*; n = 4, 8, 8, 3 cells from one, one, two, and one cultures for Archer, QuasAr2, Archon1, and Archon2, respectively) illumination. Box plots with notches are used (see caption for Fig. 1d for description). Dots, individual data points.

Supplementary Figure 18. Optical initiation and voltage imaging of action potentials in cultured primary mouse hippocampal neurons co-expressing CoChR and Archon1.

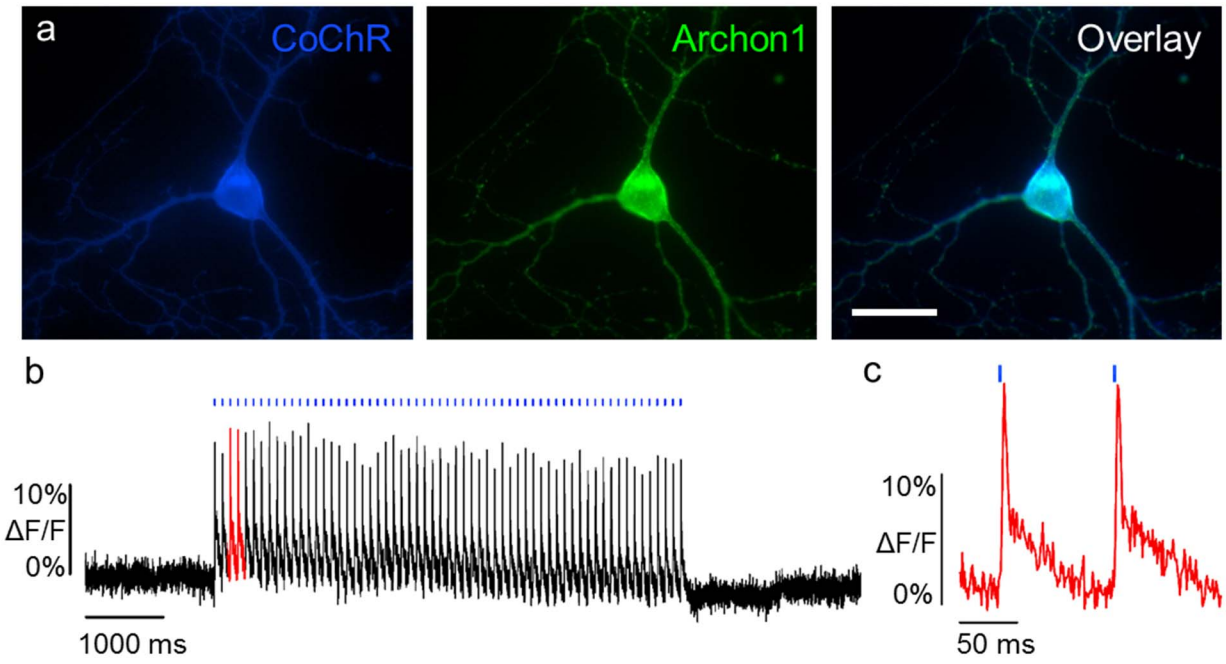

(**a**) Representative fluorescence images of a neuron co-expressing CoChR-mTagBFP2 and Archon1-EGFP (*left*; imaged via mTagBFP2 fluorescence, λ_{ex} = 377/25BP from an LED, λ_{em} = 447/60BP; *middle,* imaged via EGFP fluorescence, excitation (λ_{ex}) at 474/23BP from an LED, emission (λ_{em}) at 527/50BP; *right*, overlay of the left and middle images; n = 11 neurons from one culture). Scale bar, 25 μm. (**b**) Representative fluorescence trace of Archon1 reporting activity of the neuron shown in panel **a** and (**c**) the section of the trace in **b** highlighted in red color (n = 11 neurons from one culture). The neuronal activity was triggered by blue illumination and imaged by red excitation (blue illumination: 470/20 nm light from an LED, 10 Hz, 1 ms per pulse at 0.14 mW/mm^2, blue bars; red illumination: 637 nm laser light at 1.5 W/mm^2, λ_{em} = 664LP). The trace was acquired at the soma of the neuron with image acquisition rate of 1 kHz.

Supplementary Figure 19. Dendritic voltage imaging in cultured primary mouse hippocampal neurons.

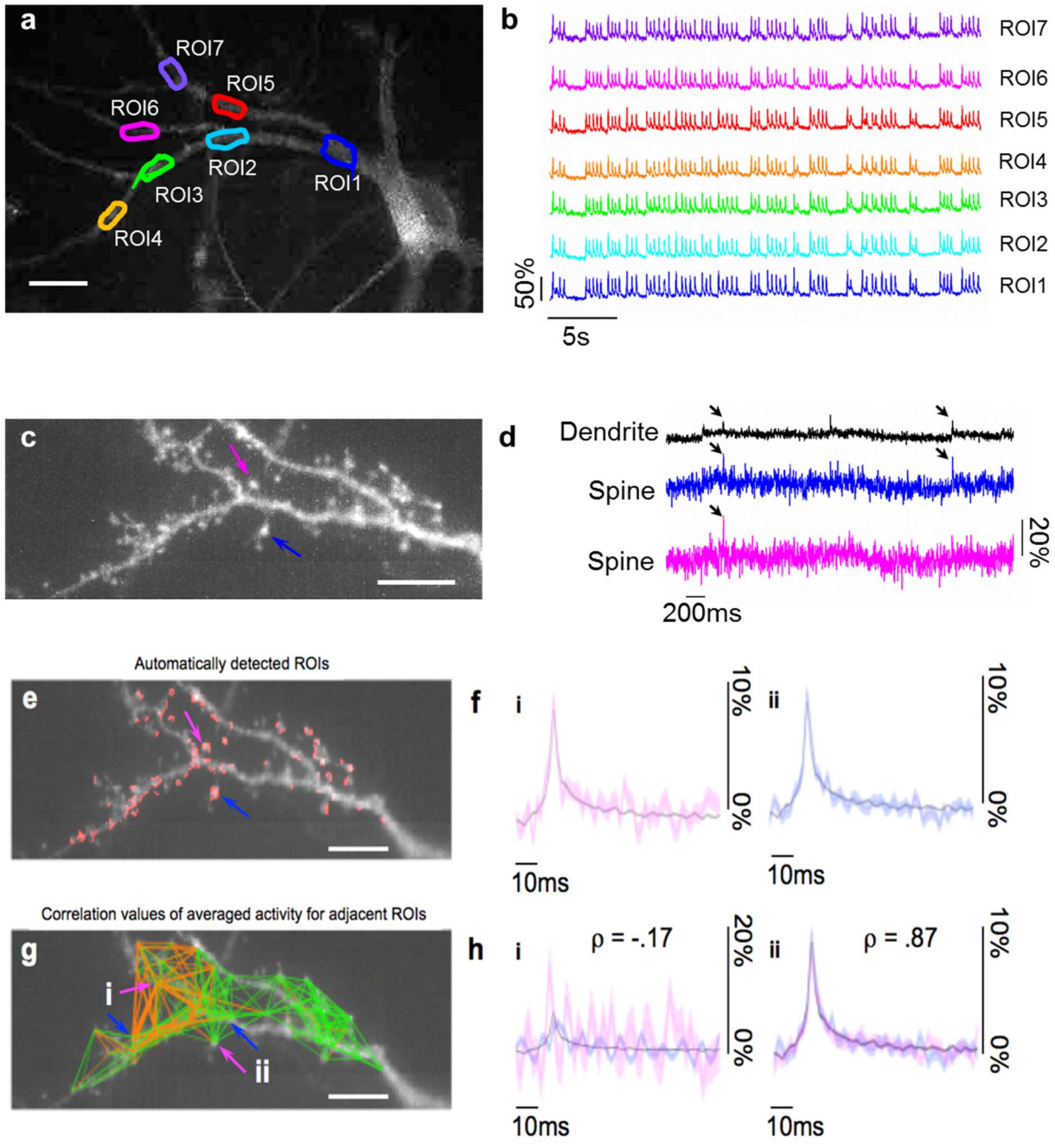

(**a**) A fluorescence image of a cultured neuron expressing Archon1 (n = 1 neuron). Excitation at 637 nm laser light, 800 mW/mm^2, emission at 664LP, image acquisition rate: 381 Hz for **a, b**. (**b**) Fluorescence traces from single-trial optical recordings of action potentials analyzed for the color-matched dendritic regions of interest (ROIs) outlined in (**a**). (**c**) A fluorescence image of dendrites of a cultured neuron expressing Archon. Arrows indicate dendritic spines referred to later in the

figure. (**d**) Fluorescence traces from single-trial optical recordings analyzed for the individual spines indicated with color-matched arrows in (**c**). Excitation at 637 nm laser light, 800 mW/mm^2, emission at 664LP, image acquisition rate: 555 Hz for **c-h.** Black trace acquired from dendritic shaft proximal to the indicated spines (n = 1 neuron). (**e**) Our computational method for identifying ROIs classifies pixels as either noise or signal via a rank-2 non-negative matrix factorization (NMF) on the power spectral density of each pixel trace. The signal or noise classification for all pixels is based on a human expert choosing a single example pixel that corresponds to clear Archon2 signal. Shown in red are the pixels determined to be Archon2 signal by the NMF algorithm and clustered into ROIs via connected components (ROIs of less than 6 pixels are excluded, see **Online Methods** for details of analysis and MATLAB code), and overlaid on a fluorescence image of the same dendrite shown in (**c**). (**f**) Overlay of averaged waveforms of fluorescence signal for peak events (n = 131 peaks exhibiting over 5% $\Delta F/F$, the selected time window per waveform starts 18 ms before peak and includes 72 ms after peak). The black trace is the averaged waveform from the sum of all ROIs in (**e**) and included as a reference in **i, ii** and again in (**h**) **i, ii**. Two representative ROIs from dendritic spines, magenta arrow (**i,** *magenta trace*) and blue arrow (**ii,** *blue trace*), are overlaid with average waveform across all ROIs (*black trace*) to show the difference between a single dendritic spine waveform and total dendritic waveform. The standard error of the mean is drawn around each averaged spine-localized trace. **(g**) Pearson correlation coefficients, ρ, calculated between pairs of averaged fluorescence traces from each ROI, such as those shown in (**f**), are visualized by drawing green lines for positive ($\rho>0$) correlation and orange lines for negative ($\rho<0$) correlation. The thickness of each line is proportional to the magnitude of correlation value and for clarity of presentation, only ROI pairs within 16μm of each other are visualized. (**h**) Pairs of averaged spike waveforms identified with color-matched arrows in (**g**) are overlaid to demonstrate a negatively correlated pair of ROIs (**i**) and a highly correlated pair of ROIs (**ii**). Scale bars, 20 μm.

Supplementary Figure 20. Expression of Archons in mouse brain.

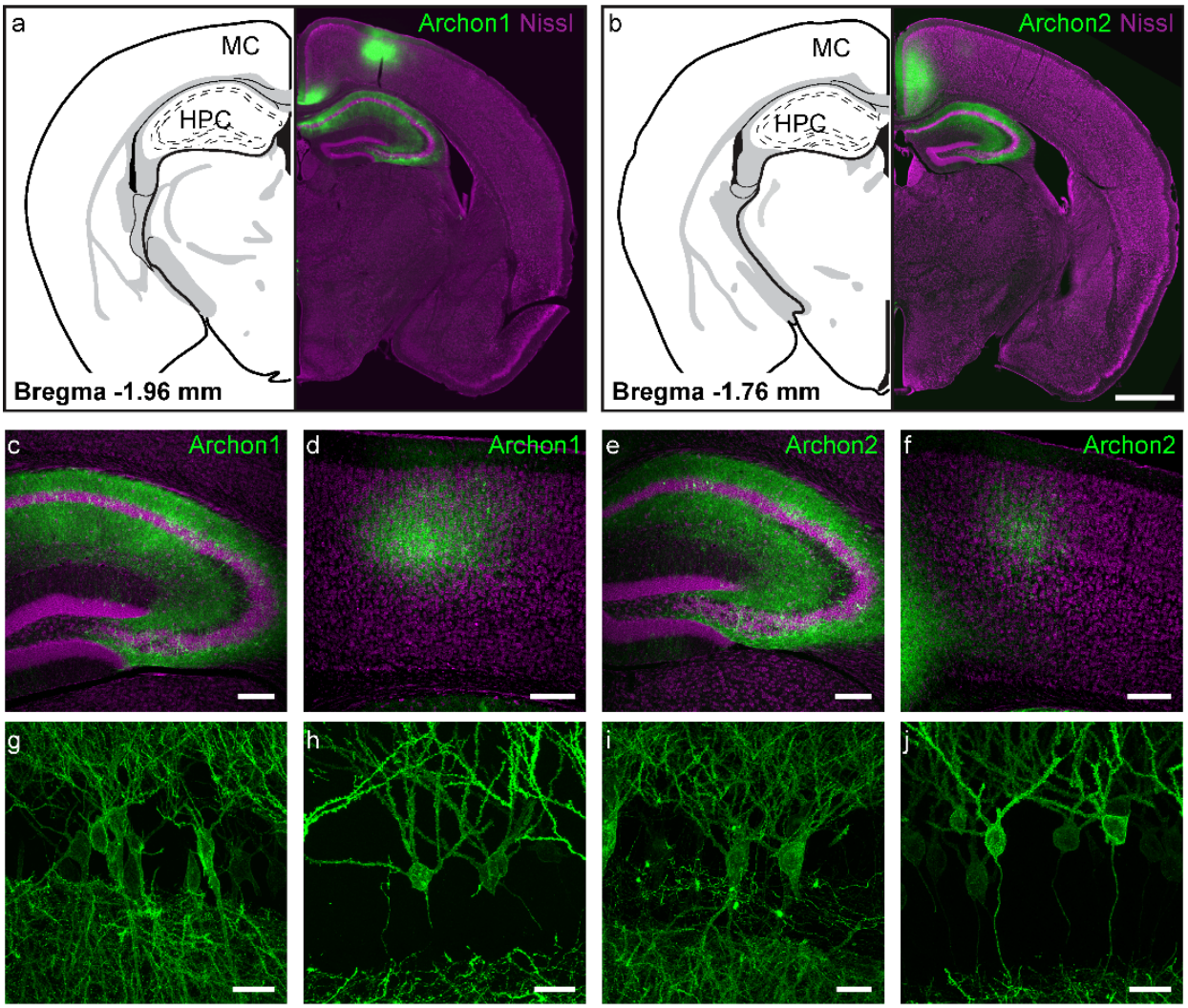

Archon1-EGFP or Archon2-EGFP were expressed in mouse brain by IUE at E15.5 and observed at postnatal day 20-30 (P20-P30). (**a-f**) Representative epi-fluorescence images from coronal sections of Archon1-EGFP (**a, c, d**) and Archon2-EGFP (**b, e, f**) expression (EGFP channel shown in green; Nissl staining is shown in magenta; direct Archon fluorescence did not survive formaldehyde fixation). (**a, b**) Whole brain overview from the hemisphere targeted by IUE (*right panel*), and the corresponding brain atlas section (adapted from *ref.* [29]), relative to bregma (*left panel*). Targeting hippocampus (HPC) by IUE at E15.5 resulted also in sparse Archon expression in L2/3 pyramidal neurons in the motor cortex (MC) of the same hemisphere (negative pole electrode), and recordings were obtained from pyramidal neurons in MC (n = 70 slices from 3 mice for each construct). (**c-f**) Higher magnification of the same images shows expression of Archon1-EGFP (**c, d**) and Archon2-EGFP (**e, f**) in HPC (**c, e**) and MC (**d, f**). Note the sparser expression of Archons in MC, allowing better optical isolation of individual cells. (**g-j**) Confocal images of Archon1-EGFP (**g, h**) and Archon2-EGFP (**i, j**) -expressing pyramidal neurons (**g, i**) and dentate gyrus granule cells (**h, j**) in hippocampus. Scale bars, 1 mm (**a, b**), 200 µm (**c-f**), and 25 µm (**g-j**).

Supplementary Figure 21. Membrane properties of neurons in mouse brain slice under red light illumination.

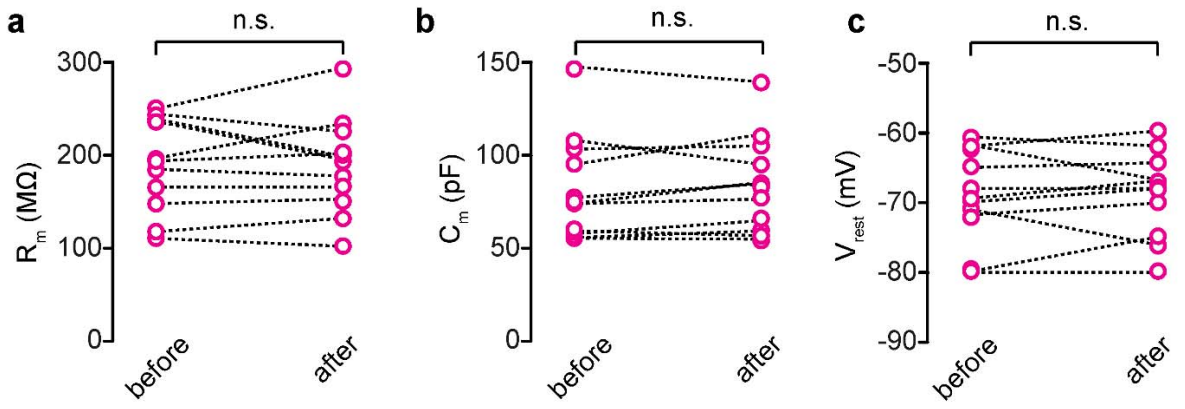

Quantification of membrane resistance R_m (**a**), membrane capacitance C_m (**b**), and resting potential V_{rest} (**c**) from Archon1-expressing pyramidal neurons in L2/3 mouse brain slice before and after illumination (λ_{ex} = 637 nm laser light at 15 W/mm^2; cumulative illumination duration ranged from 30 to 200 seconds per cell; n = 11 neurons from 6 mice). Dashed lines connect data points from the same neuron. No obvious change in membrane properties was noticed (P = 0.89 for R_m, P = 0.67 for C_m, and P = 0.79 for V_{rest}; Wilcoxon rank sum test).

Supplementary Figure 22. Membrane localization of Archon1 in mouse brain.

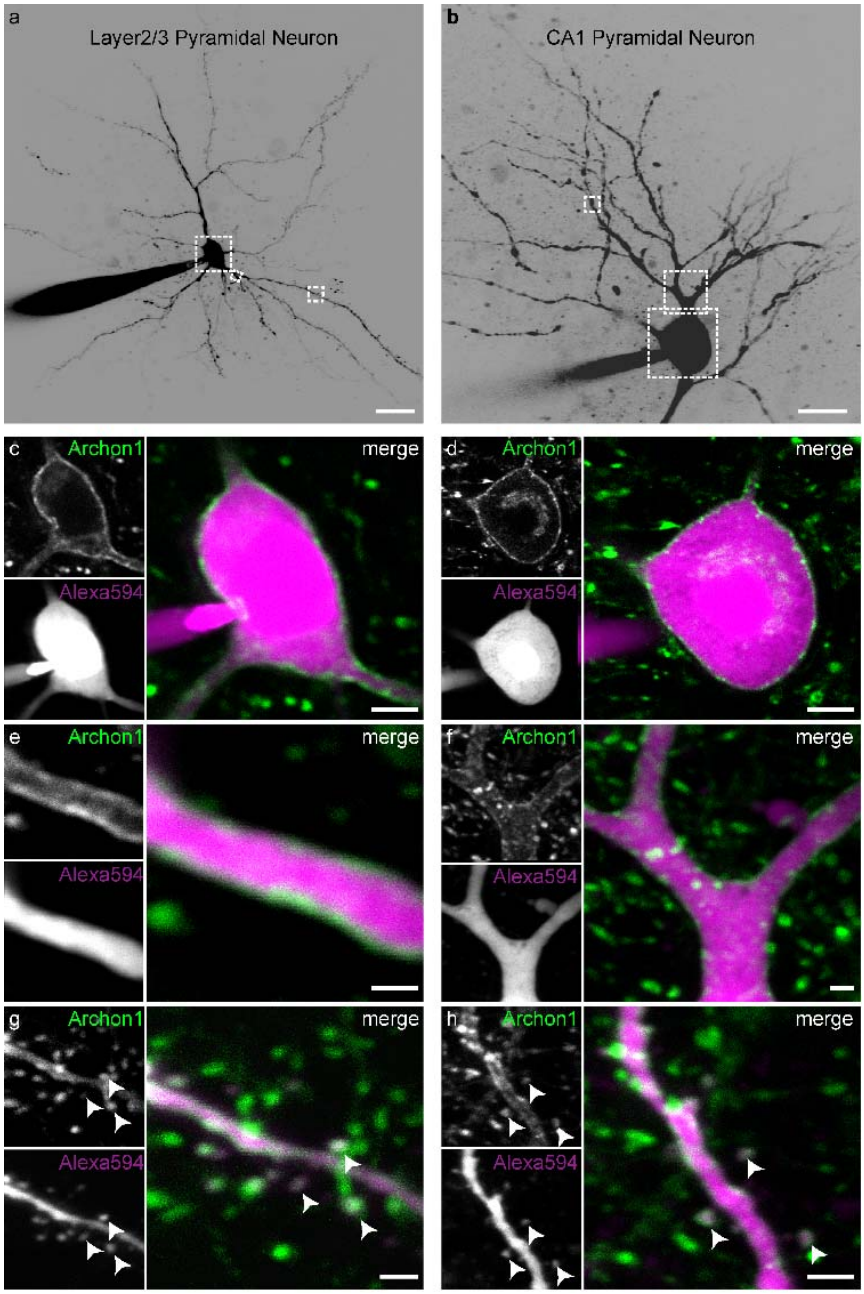

Representative two-photon images of pyramidal neurons in cortex L2/3 (*left*) and hippocampus CA1 (*right*) expressing Archon1-EGFP in acute brain slices; shown is the EGFP channel (see **Supp. Fig. 20** for details). (**a, b**) Low-magnification overview of cells filled through the recording pipette with Alexa Fluor 594. Images represent maximum projections of z-stacks; boxes indicate regions shown below at higher magnification from individual z-planes (n = 10 slices from 2 mice). (**c-f**) Archon1-EGFP (*green*) was enriched at the cell surface, both at the soma (**c, d**) and in spiny, proximal dendrites (**e, f**). In contrast, soluble Alexa Fluor 594 (Alexa594, *magenta*) filled the cell homogeneously. (**g, h**) Archon1-EGFP was also readily detected at spine-heads in more distal dendrites (*arrowheads*). Scale bars are 25 µm (**a, b**), 5 µm (**c, d**), and 2 µm (**e-h**).

Supplementary Figure 23. Expression of QuasAr2 and Archer1 in mouse brain.

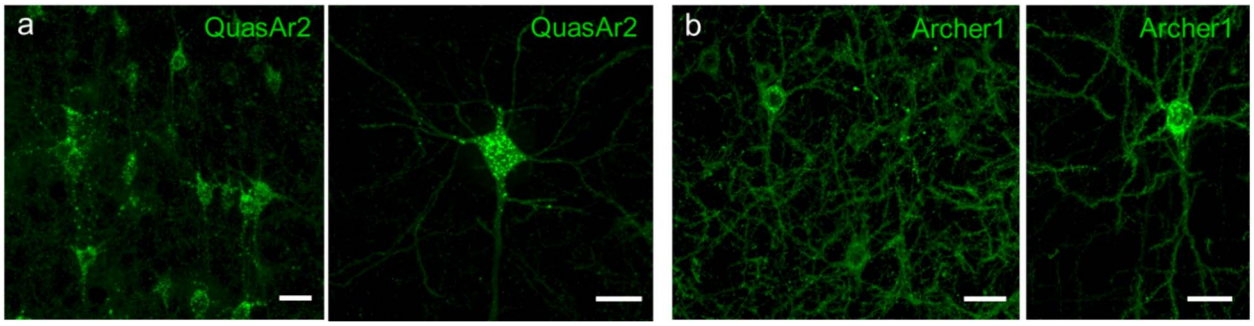

QuasAr2-mOrange or Archer1-EGFP were expressed in mouse brain by IUE at E15.5 and observed at P22. Images were obtained from L2/3 neurons in coronal sections of motor cortex (MC). (**a**) Representative confocal images of QuasAr2-mOrange expressing neurons in MC (imaged via mOrange2 fluorescence; n = 8 slices from 2 mice). (**b**) Representative confocal images of Archer1-EGFP expressing neurons in MC (imaged via EGFP fluorescence; n = 8 slices from 2 mice). Direct QuasAr2 and Archer1 fluorescence did not survive formaldehyde fixation. Scale bars, 25 μm.

Supplementary Figure 24. Voltage imaging of Archon1 in mouse brain slice.

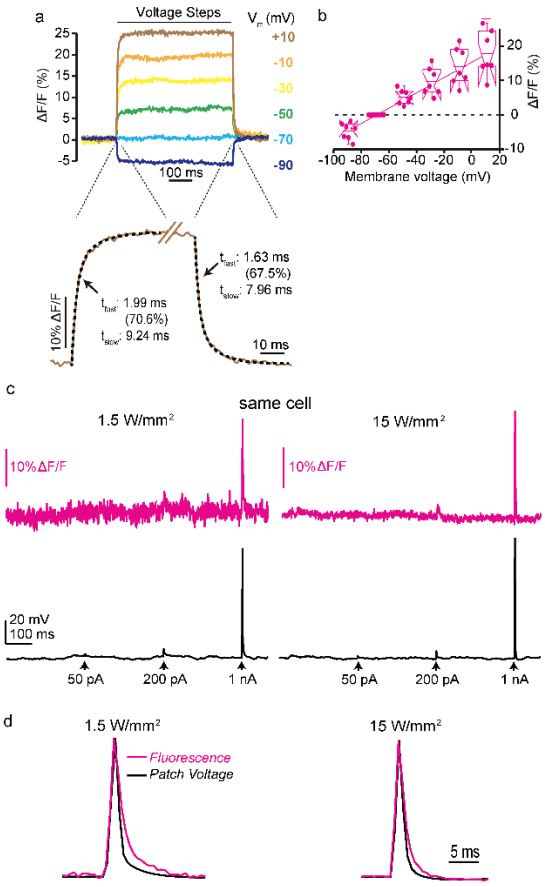

Archon1-expressing pyramidal neurons in layer (L) 2/3 of motor cortex were targeted by patch-clamp recording, and Archon fluorescence at the soma was imaged at 1 kHz. Excitation intensity was ~7 mW over the area of the soma (*i.e.*, ~15 W/mm^2 at 637 nm, but 10x lower intensity, 1.5 W/mm^2 at 637nm, was used in panels **c**, **d** for comparison to the high illumination condition). (**a**) Representative traces of voltage imaging recordings for a series of hyper- and depolarizing voltage steps in voltage-clamp mode in a neuron expressing Archon1 (*top*). Rise and decay phases of the voltage step from -70 to +10 mV are shown on extended time scales (*bottom, brown solid line*), overlaid with the fit to a double-exponential function to determine rise and decay kinetics (*black dotted line*). Numbers are as in **Fig. 2c**. (**b**) Population data corresponding to the experiment of **a** (n = 7 neurons from 2 mice). Box plots with notches are used (see caption for **Fig. 1d** for description). Data was normalized so that -70 mV was set to 0 ΔF/F (and hence appears as a collapsed box). (**c**) Simultaneous Archon fluorescence imaging (*top, magenta*) and whole-cell current-clamp patch recording (*bottom, black*) during injection of current pulses with increasing amplitude (50 pA, 200 pA, and 1 nA, 2 ms; *arrows*). Shown are 1-second long sweeps from one Archon1 expressing cell first with 1.5 W/mm^2 (*left*) and then with 15 W/mm^2 (*right*) excitation light. (**d**) Overlay of averaged action potential voltage waveform (*black*) and fluorescent signal from Archon1 (*magenta*), scaled to peak (from n = 30 sweeps from one cell), and recorded at 1.5 W/mm^2 (*top*) and 15 W/mm^2 (*bottom*) excitation light.

Supplementary Figure 25. Voltage imaging of Archon2 in mouse brain slice.

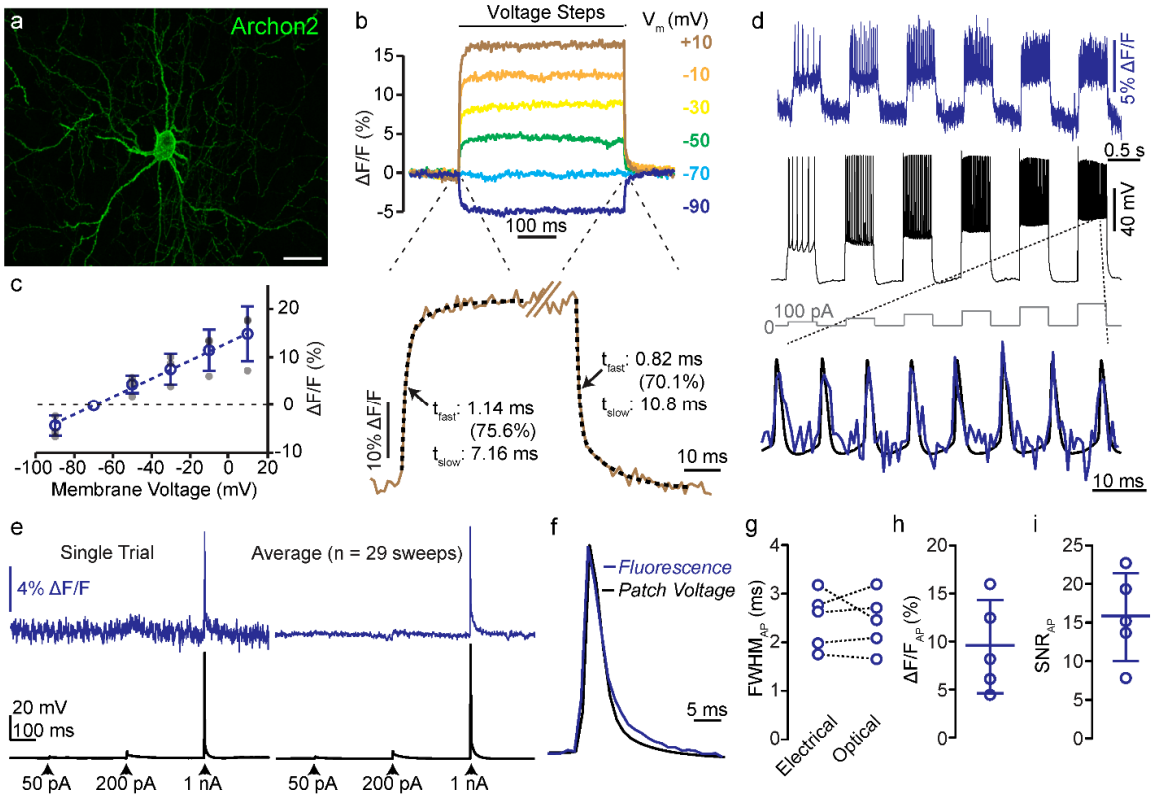

Archon2 expressing pyramidal neurons in L2/3 of motor cortex were targeted by patch clamp recordings, and Archon fluorescence at the soma was imaged simultaneously with an EMCCD camera at 1 kHz. Excitation intensity was ~7 mW over the area of the soma (*i.e.*, ~15 W/mm^2 at 637 nm. (**a**) Representative image of Archon2-EGFP expression in L2/3 pyramidal neurons (n = 70 slices from 3 mice). Scale bar, 25 µm. (**b**) Representative traces of voltage imaging recordings for a series of hyper- and depolarizing voltage steps in voltage-clamp mode in a neuron expressing Archon2 (*top*). Rise and decay phases of the voltage step from -70 to +10 mV are shown on extended time scales (*bottom, brown solid line*), overlaid with the fit to a double-exponential function to determine the rise and decay kinetics (*black dotted line*). Numbers are as in **Fig. 2c**.(**c**) Population data corresponding to the experiment of **b** (n = 3 neurons from 1 mouse; individual data points in gray dots). Open circles: mean; error bars: standard deviation. (**d**) A series of 500 ms current steps with increasing amplitudes (from 100 to 600 pA in 100 pA steps; *gray line*) were injected through the recording pipette, resulting in action potentials of varying frequency. (**e**) Simultaneous Archon2 fluorescence imaging (*top, blue*) and whole-cell current-clamp patch recording (*bottom, black*) during injection of current pulses with increasing amplitude (50 pA, 200 pA, and 1 nA, 2 ms; arrows). Shown are 1-second long sweeps from Archon2 expressing cells, from both single trials (*left*) and averaged over 29 sweeps from the same cell (*right*). (**f**) Overlay of the averaged action potential current waveform (*black*) and fluorescent signal from Archon2 (*blue*), scaled to peak (from n = 29 sweeps from one cell). (**g-i**) Quantification of electrical and optical full width at half maximum (FWHM; dashed lines connect data points from the same neuron) (**g**), ΔF/F (**h**), and SNR (**i**) across all recordings (n = 5 neurons from 2 mice), for action potentials. In **g-i** open circles represent individual neurons; in **h** and **i** bars indicated mean ± standard derivation.

Supplementary Figure 26. Voltage imaging of putative subthreshold events using zArchon1 in larval zebrafish.

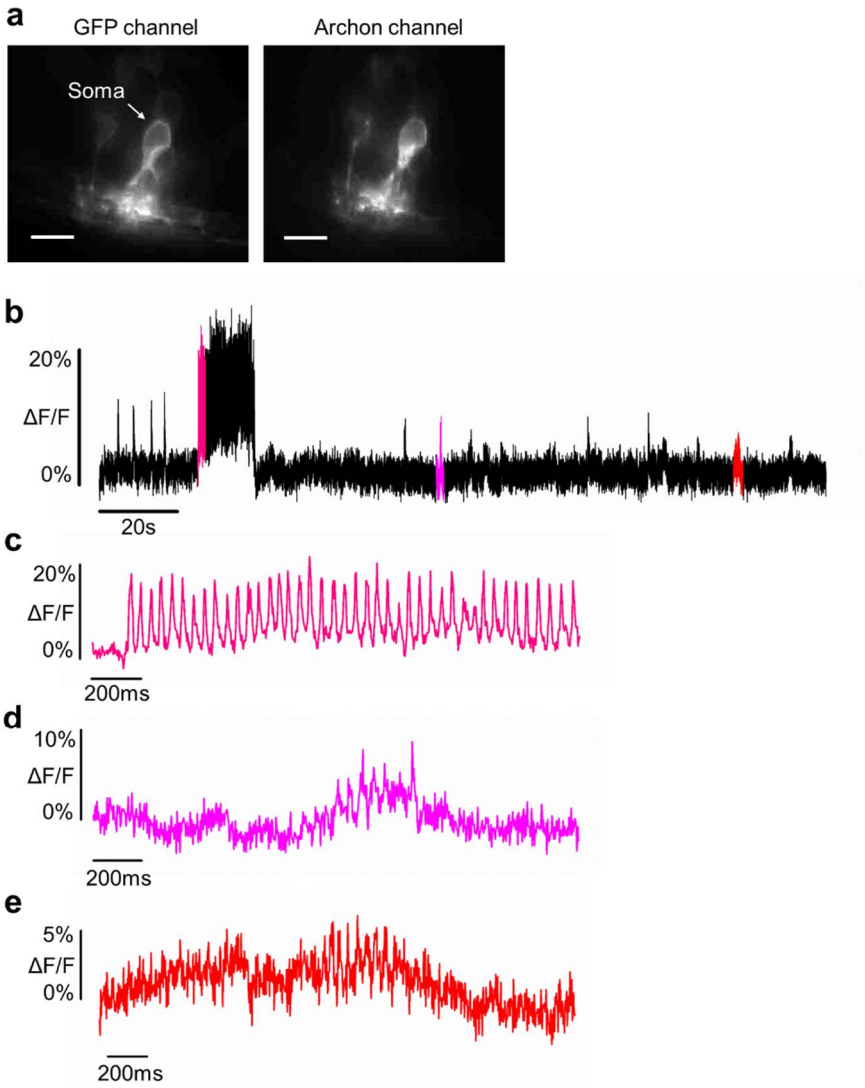

(**a**) Representative image of a neuron expressing zArchon1-EGFP in the spinal cord of a zebrafish larva at 4 days post fertilization (dpf) immobilized in agarose under wide-field microscopy in the GFP channel (*left*; excitation (λ_{ex}) at 474/23BP from an LED, emission (λ_{em}) at 527/50BP) and the Archon channel (*right*; λ_{ex} = 637 nm laser light, λ_{em} = 664LP; n = 6 neurons in 6 fish). Scale bar, 10 µm. (**b**) Representative fluorescence trace of zArchon1-EGFP reporting spontaneous activity of the neuron shown in **a** (n = 6 neurons in 6 fish). The trace was acquired at the soma of the neuron (λ_{ex} = 637 nm at 2.2 W/mm^2, λ_{em} = 664LP, image acquisition rate: 333 Hz). (**c**,**d**,**e**) The sections of **b** highlighted in matched colors, shown at expanded time scales.

Supplementary Figure 27. Photostability of zArchon1 in larval zebrafish.

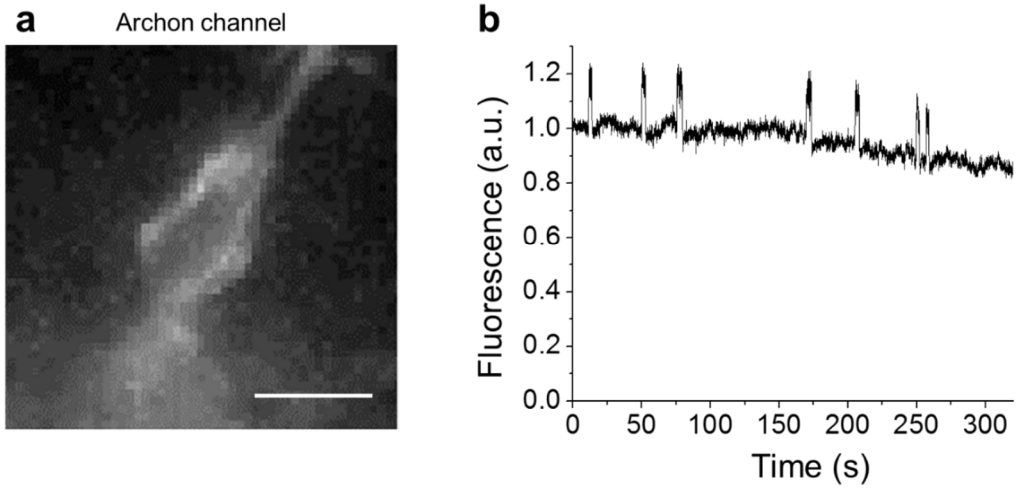

(**a**) Representative image (excitation (λ_{ex}) at 637 nm laser light, emission (λ_{em}) at 664LP, i.e. the Archon channel) of a neuron expressing zArchon1 in a zebrafish larva at 4 days post fertilization (dpf) immobilized in agarose under wide-field microscopy (n = 11 neurons in 6 fish). Scale bar, 10 μm. (**b**) Representative fluorescence trace of zArchon1 reporting spontaneous activity of the neuron shown in panel **a** (n = 11 neurons in 6 fish). The trace was acquired at the soma of the neuron over 300 seconds of continuous illumination (λ_{ex} = 637 nm laser light at 2.2 W/mm^2, λ_{em} = 664LP; image acquisition rate: 25 Hz).

Supplementary Figure 28. Membrane localization of wArchon1 in *C.elegans*.

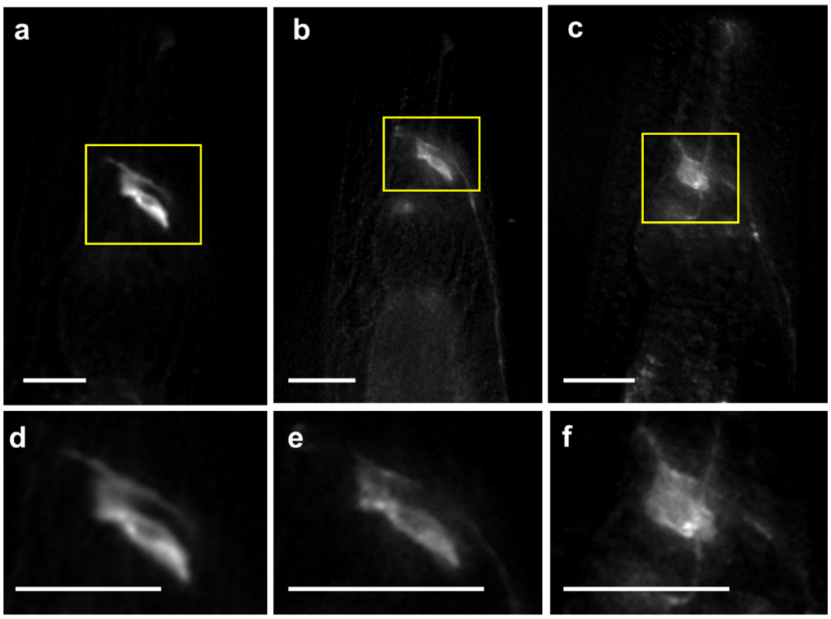

(**a-f**) Representative fluorescence images of *C. elegans* expressing wArchon1 in AVA neurons (n = 40 worms). (**d-f**) Magnified views of the AVA neuron somas in the boxed regions of **a-c**, respectively. The fluorescence images were acquired using 637 nm laser light excitation and a 664LP emission filter. Scale bars, 20 μm.

Supplementary Figure 29. Voltage imaging in *C.elegans* using wArchon1.

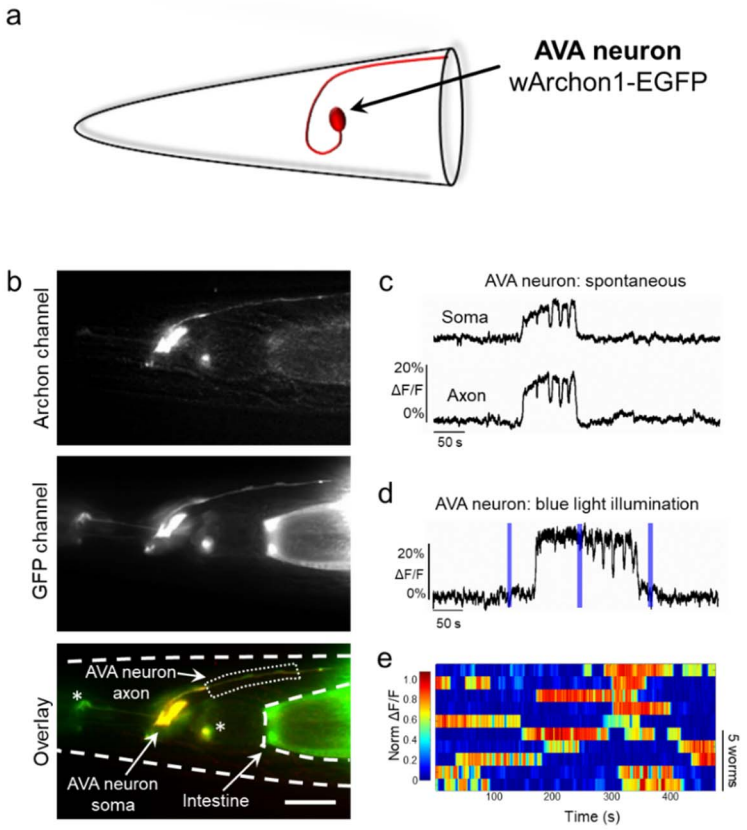

(**a**) Schematic of AVA neuron expressing *C. elegans* codon-optimized fusion of Archon1 (or wArchon1 for short) with EGFP (red) in the head of *C. elegans*. (**b**) Representative fluorescence images of *C. elegans* head expressing wArchon1-EGFP under control of the *rig-3* promoter. Shown is fluorescence in an AVA neuron (top, Archon channel (excitation (λ_{ex}) at 637 nm laser light, emission (λ_{em}) at 664LP); middle, GFP channel (λ_{ex} = 475/34BP from an LED and λ_{em} = 527/50BP); bottom, overlay, with Archon in red and GFP in green), as well as in pharyngeal neurons that also express under control of the *rig-3* promoter (asterisks). AVA neuron soma and axon are indicated (n = 10 worms). Scale bar: 10 µm. (**c**) The AVA neurons, when imaged at points at the soma or along the axon, exhibited long-lasting (tens of seconds to several minutes) high and low states similar to those previously reported in AVA calcium recordings[30], with changes in fluorescence intensity relative to baseline of magnitude ~20-25% and SNR ~25-35 (although the diversity of these fluctuations, in contrast to the stereotyped action potentials of vertebrate neurons, makes it difficult to arrive at a single number). Panel **c** shows representative fluorescence traces of wArchon1 reporting spontaneous activity in soma (top) and axon (bottom) of an AVA neuron. Imaging conditions: λ_{ex} = 637 nm laser light at 800mW/mm^2, λ_{em} = 664LP; image acquisition rate: 33 Hz, were used throughout the figure for Archon imaging (n = 10 cells from 10 worms). (**d**) Blue light illumination (three pulses of 6 sec duration each) did not affect wArchon1 fluorescence in either high or low voltage states. A representative trace of wArchon1 fluorescence in the soma of an AVA neuron under three pulses of blue light illumination (0.2 mW/mm^2, λ_{ex} = 475/34BP from an LED, 6 s; blue bars; n = 10 cells from 10 worms). (**e**) Individual traces of wArchon1 fluorescence in AVA neurons under blue light illumination (n=10 neurons in 10 worms).

Supplementary References:

1. Hochbaum, D. R. *et al.* All-optical electrophysiology in mammalian neurons using engineered microbial rhodopsins. *Nat. Methods* **11,** 825–33 (2014).
2. Flytzanis, N. C. *et al.* Archaerhodopsin variants with enhanced voltage-sensitive fluorescence in mammalian and Caenorhabditis elegans neurons. *Nat. Commun.* **5,** 4894 (2014).
3. Gong, Y. *et al.* High-speed recording of neural spikes in awake mice and flies with a fluorescent voltage sensor. *Sciencexpress* **350,** 1–11 (2015).
4. Wagner, M. J., Li, J. Z., Gong, Y. & Schnitzer, M. J. FRET-opsin protein voltage sensors. *Nat. Commun.* **5,** 1–11 (2014).
5. St-Pierre, F. *et al.* High-fidelity optical reporting of neuronal electrical activity with an ultrafast fluorescent voltage sensor. *Nat. Neurosci.* **17,** 884–9 (2014).
6. Tsutsui, H. *et al.* Improved detection of electrical activity with a voltage probe based on a voltage-sensing phosphatase. *J Physiol* **591,** 4427–4437 (2013).
7. Akemann, W. *et al.* Imaging neural circuit dynamics with a voltage-sensitive fluorescent protein. *J Neurophysiol* **108,** 2323–2337 (2012).
8. Zou, P. *et al.* Bright and fast multicoloured voltage reporters via electrochromic FRET. *Nat. Commun.* **5,** 4625 (2014).
9. Shaner, N. C. *et al.* A bright monomeric green fluorescent protein derived from Branchiostoma lanceolatum. *Nat. Methods* **10,** 407–409 (2013).
10. Yang, H. H. H. *et al.* Subcellular Imaging of Voltage and Calcium Signals Reveals Neural Processing In??Vivo. *Cell* **166,** 245–257 (2016).
11. Shcherbakova, D. M. & Verkhusha, V. V. Near-infrared fluorescent proteins for multicolor in vivo imaging. *Nat. Methods* **10,** 751–754 (2013).
12. Yu, D. *et al.* A naturally monomeric infrared fluorescent protein for protein labeling in vivo. *Nat. Methods* **12,** 763–5 (2015).
13. Shcherbakova, D. M. *et al.* Bright monomeric near-infrared fluorescent proteins as tags and biosensors for multiscale imaging. *Nat. Commun.* **7,** 1–12 (2016).
14. Heiser, W. C. Optimizing Electroporation conditions for the Transformation of Mammalian Cells. *Methods Mol Biol.* **130,** (2000).
15. Reid, L. H., Shesely, E. G., Kim, H. & Al, R. E. T. Cotransformation and Gene Targeting

in Mouse Embryonic Stem Cells. **11,** 2769–2777 (1991).

16. Kutner, R. H., Zhang, X.-Y. & Reiser, J. Production, concentration and titration of pseudotyped HIV-1-based lentiviral vectors. *Nat. Protoc.* **4,** 495–505 (2009).
17. Wang, L. & Tsien, R. Y. Evolving proteins in mammalian cells using somatic hypermutation. *Nat. Protoc.* **1,** 1346–1350 (2006).
18. Jordan, M., Schallhorn, A., Wurm, F. M. & Francisco, S. S. Transfecting mammalian cells : optimization of critical parameters affecting calcium-phosphate precipitate formation. **24,** 596–601 (1996).
19. Jordan, M. & Wurm, F. Transfection of adherent and suspended cells by calcium phosphate. *Methods* **33,** 136–143 (2004).
20. Mahon, M. J. Vectors bicistronically linking a gene of interest to the SV40 large T antigen in combination with the SV40 origin of replication enhance transient protein expression and luciferase reporter activity. *Biotechniques* **51,** 119–126 (2011).
21. Giraud, E. *et al.* Bacteriophytochrome controls photosystem synthesis in anoxygenic bacteria. *Nature* **417,** 202–205 (2002).
22. Piatkevich, K. D., Subach, F. V & Verkhusha, V. V. Engineering of bacterial phytochromes for near-infrared imaging, sensing, and light-control in mammals. *Chem. Soc. Rev.* **42,** 3441–52 (2013).
23. Lebkowski, J. S., DuBridge, R. B., Antell, E. a, Greisen, K. S. & Calos, M. P. Transfected DNA is mutated in monkey, mouse, and human cells. *Mol. Cell. Biol.* **4,** 1951–1960 (1984).
24. Razzaque, A., Mizusawa, H. & Seidman, M. M. Rearrangement and mutagenesis of a shuttle vector plasmid after passage in mammalian cells. *Proc. Natl. Acad. Sci. U. S. A.* **80,** 3010–3014 (1983).
25. Környei, Z. *et al.* Cell sorting in a Petri dish controlled by computer vision. *Sci. Rep.* **3,** 1088 (2013).
26. Bellini, D. & Papiz, M. Z. Structure of a bacteriophytochrome and light-stimulated protomer swapping with a gene repressor. *Structure* **20,** 1436–1446 (2012).
27. Ai, H.-W., Baird, M. A., Shen, Y., Davidson, M. W. & Campbell, R. E. Engineering and characterizing monomeric fluorescent proteins for live-cell imaging applications. *Nat. Protoc.* **9,** 910–28 (2014).

28. Piatkevich, K. D. *et al.* Near-Infrared Fluorescent Proteins Engineered from Bacterial Phytochromes in Neuroimaging. *Biophys. J.* **113,** 2299–2309 (2017).
29. Paxinos, G. & Franklin, K. B. J. *The mouse brain in stereotaxic coordinates*. *Academic Press* **2nd,** (2004).
30. Gordus, A. *et al.* Feedback from Network States Generates Variability in a Probabilistic Olfactory Circuit. *Cell* **161,** 215–227 (2015).